

001  
002  
003  
004  
005  
006  
007  
008  
009  
010  
011  
012  
013  
014  
015  
016  
017  
018  
019  
020  
021  
022  
023  
024  
025  
026  
027  
028  
029  
030  
031  
032  
033  
034  
035  
036  
037  
038  
039  
040  
041  
042  
043  
044  
045  
046

# The Importance of Initial Conditions in Seasonal Predictions of Antarctic Sea Ice

Elio Campitelli<sup>1,2\*</sup>, Ariaan Purich<sup>1,2</sup>, Julie Arblaster<sup>1,2</sup>,  
Eun-Pa Lim<sup>3</sup>, Matthew C. Wheeler<sup>3</sup>, Phillip Reid<sup>3</sup>

<sup>1</sup>School of Earth, Atmosphere and Environment, Monash University, Kulin  
Nations, Clayton, Victoria, Australia..

<sup>2</sup>SARC Special Research Initiative for Securing Antarctica's  
Environmental Future, Clayton, Kulin Nations, Victoria, Australia.

<sup>3</sup>Research, Bureau of Meteorology, Australia.

\*Corresponding author(s). E-mail(s): [elio.campitelli@monash.edu](mailto:elio.campitelli@monash.edu);

## Abstract

Accurate Antarctic sea-ice forecasts are crucial for climate monitoring and operational planning, yet they remain challenging due to model biases and complex ice-ocean-atmosphere interactions. The two versions of the Australian Bureau of Meteorology's ACCESS seasonal forecast system, ACCESS-S1 and ACCESS-S2, use identical model configuration and differ only in their initial conditions; primarily in that ACCESS-S2 does not assimilate sea-ice observations, whereas ACCESS-S1 does.

This provides a convenient opportunistic experiment to assess the role of initial conditions on Antarctic sea-ice forecasts using more than 20 years of fully coupled simulations with two 9-member ensembles. Our analysis reveals that both systems experience an extended melt season and delayed growth phase compared with observations. This leads to a significant negative sea-ice extent bias, which is corrected only in ACCESS-S1 by the data assimilation system. The impact of the differing initial conditions on forecast errors varies dramatically by season: summer and autumn initial conditions (January-April) provide predictive skill for up to three months, with February initial conditions being particularly crucial.

047 In contrast, winter forecasts of the two systems are statistically indistinguishable  
048 after only two weeks. Regional analysis of forecast skill suggests that this  
049 winter predictability barrier is most dramatic over East Antarctica, where even  
050 ACCESS-S1 shows negative skill. These findings highlight the critical importance  
051 of comprehensive year-round sampling in predictability studies and suggest that  
052 operational sea-ice data assimilation efforts should prioritize the summer-autumn  
053 period when initial conditions have maximum impact on forecast skill.

054  
055 **Keywords:** sea ice, seasonal predictability, initial conditions, forecasting

056  
057  
058  
059

## 060 **Introduction**

061

062 Accurately modelling Antarctic sea ice is essential for understanding processes and  
063 improving climate projections to inform adaptation strategies. Accurate seasonal to  
064 sub-seasonal forecasts are also crucial for operation contingency planning in and  
065 around the Antarctic continent, including scientific missions, fisheries, and tourism<sup>1;2</sup>.  
066

067 Improvements in modelled sea-ice might also help improve weather forecasts over and  
068 away from sea-ice regions<sup>3–5</sup>.

069

070 However, progress in Antarctic sea-ice forecasting system has lagged behind Arctic  
071 sea-ice forecasts due to model biases, and inherent large variability and complexity<sup>6;7</sup>.  
072

073 Dynamical seasonal forecasts of summer Antarctic sea ice have been shown to perform  
074 worse than relatively simpler statistical methods<sup>8</sup> and machine learning approaches (e.g.  
075 Dong et al.<sup>9</sup>, Lin et al.<sup>10</sup>), which also underscores the need for better understanding  
076 and physical modelling of sea-ice dynamics, and drivers of its variability.

077

078 Good initial conditions are generally required for a good forecast, however, it is not  
079 entirely known to what extent accurate sea-ice initial conditions affect the quality of  
080 the forecast and at what timescales. Exploring seasonal predictions of Arctic sea ice,  
081 Guemas et al.<sup>11</sup> found that sea-ice initial conditions are important in autumn to predict  
082 summer sea ice, but the impact wasn't as dramatic when predicting winter sea ice. Day  
083

084

et al.<sup>12</sup> also found seasonally-varying differences in the effect of initialisation, noting that accurate Arctic sea-ice thickness leads to improved sea-ice forecasts initialised in July but not when initialised in January.

For the Antarctic, Holland et al.<sup>13</sup> studied the initial-value predictability of Antarctic sea ice in a perfect model study using the CCSM3 model. They found that sea-ice and ocean initial conditions provide predictive information to forecast sea-ice edge location several months in advance and that some predictability is retained for up to two years thanks to ocean heat content anomalies that are advected eastward. This is in contrast with Marchi et al.<sup>14</sup>, who ran perfect model experiments to argue that uncertainty in the predicted atmospheric state and evolution is the main driver of uncertainty in Antarctic sea-ice extent prediction on seasonal timescales, with sea-ice and ocean initial conditions having lesser importance. More recently, Morioka et al.<sup>15</sup> studied decadal forecasts of Antarctic sea ice and found that initialising ocean and sea ice improved the correlation between simulated and observed sea-ice concentration evolution in the Amundsen–Bellingshausen Sea. It is hard to compare these studies since they are based on forecasts initialised at different times of the year and different frameworks: Holland et al.<sup>13</sup> ran 20 ensemble members initialised on the 1st of January of a particular year, Marchi et al.<sup>14</sup> ran forecasts from the 1st of March and 1st of September, and Morioka et al.<sup>15</sup> ran forecasts only from the 1st of March. Marchi et al.<sup>14</sup> also used a coupled ocean–sea-ice model instead of a fully coupled model like Holland et al.<sup>13</sup> did. Morioka et al.<sup>15</sup> used observed sea-ice initial conditions and compared with observations, while Marchi et al.<sup>14</sup> and Holland et al.<sup>13</sup> were perfect model studies.

In October 2021 the Australian Bureau of Meteorology (BoM) upgraded the Australian Community Climate and Earth System Simulator – Seasonal (ACCESS-S) from version S1 to S2. While the base model remained the same, the change in version was focused on using ocean, sea-ice and land initial conditions generated by the BoM instead of depending on the UK Met Office. Crucially, compared to ACCESS-S1, ACCESS-S2

139 does not assimilate sea-ice observations, so sea ice is only affected by the ocean and  
140 atmospheric data assimilation via the coupled integration.  
141

142 Since model configuration is identical between ACCESS-S1 and ACCESS-S2, they  
143 form a sort of “opportunistic experiment” where the same forecasting model was run  
144 over a long period of time with multiple ensemble forecasts initialised throughout the  
145 year, with the only difference being the initial conditions. This provides an opportunity  
146 to test the effect of sea-ice initial conditions on the forecast of sea-ice concentrations  
147 and the climate.  
148

149 In this study we compare sea-ice hindcasts produced by ACCESS-S1 and ACCESS-S2.  
150 We focus on seasonality of errors and biases and the effect of the data assimilation  
151 system. This comparison will inform future work with the prediction system as a  
152 research tool to better understand the dynamics and variability of the Antarctic sea  
153 ice and its impacts on the climate system as well as to explore the potential of using  
154 its sea-ice forecasts for decision-making. The work will also serve as a benchmark for  
155 future prediction systems to attempt to improve upon.  
156

## 166 **Data and methods**

### 167 **ACCESS-S2**

168 ACCESS-S2<sup>16</sup> is the Bureau of Meteorology’s seasonal forecast system which became  
169 operational in October 2021, replacing the ACCESS-S1 system<sup>17</sup>. The model com-  
170 ponents of both ACCESS-S2 and ACCESS-S1 are identical with the same numbers  
171 of levels and resolution. They consist of the Global Atmosphere 6.0 (GA6)<sup>18;19</sup>, the  
172 Unified Model’s Global Land 6.0<sup>19;20</sup>, NEMO Global Ocean 5.0<sup>21;22</sup> and Global Sea  
173 Ice 6.0 [CICE; Rae et al. <sup>23</sup>]. The atmosphere has a N216 horizontal resolution (~60 km  
174 in the mid-latitudes) with 85 vertical levels. The land model uses the same horizontal  
175

grid as the atmosphere with four soil levels. The ocean component has a nominal horizontal resolution of  $1/4^\circ$  with 75 vertical levels. The sea-ice component, based on CICE version 4.1, has the same resolution as the ocean component and five sea-ice thickness categories as well as an open water category. 185  
186  
187  
188  
189  
190  
191  
192  
193  
194  
195  
196  
197  
198  
199  
200  
201  
202  
203  
204  
205  
206  
207  
208  
209  
210  
211  
212  
213  
214  
215  
216  
217  
218  
219  
220  
221  
222  
223  
224  
225  
226  
227  
228  
229  
230

Both systems take atmospheric initial conditions derived from ERA-interim<sup>24</sup> for their hindcasts. The main difference between the hindcasts of the two systems are the ocean and sea-ice initial conditions. ACCESS-S1's ocean and sea-ice initial conditions come from the Met Office FOAM system, which uses a multivariate, incremental three-dimensional variational (3D-Var), first-guess-at-appropriate-time (FGAT) data assimilation scheme<sup>25</sup> and assimilates sea surface temperature (SST), sea surface height (SSH), in situ temperature and salinity profiles, and satellite observations of sea-ice concentration using the EUMETSAT OSISAF product described in the next section. ACCESS-S2, on the other hand, is initialised from ocean conditions generated by the BoM weakly coupled ensemble data assimilation scheme described in Wedd et al.<sup>16</sup>. This scheme uses an optimal interpolation method and assimilates temperature and salinity profiles from EN4<sup>26</sup>. SSTs are nudged to Reynolds OISSTv2.1<sup>27</sup> in areas where SSTs are over  $0^\circ\text{C}$  and Sea Surface Salinity is weakly nudged to the World Ocean Atlas 2013 climatology<sup>28</sup>.

Of most relevance for this work, sea-ice concentrations are not assimilated in ACCESS-S2. Assimilation cycles are performed daily. The coupled model runs for 24 hours initialised from the previous cycle. Then the restart file fields of the ocean component are used as first guess in the data assimilation cycle and the innovations are used to build the next ocean initial conditions for the following cycle. The atmosphere fields from that daily integration are not used and instead the model atmosphere is initialised using ERA-Interim. The sea-ice initial conditions for the next cycle are the unaltered output of the previous daily integration. Then the cycle starts again and the coupled model runs for another 24 hours. During this integration the sea-ice component is

231 affected by the ocean innovations and the new atmosphere initial conditions via the  
232 coupler.

234  
235 The ACCESS-S1 hindcast set is made up of nine members created by perturbing the  
236 atmospheric fields only with a random field perturbation<sup>17</sup> and runs for 217 days for  
237 the period 1990–2012 initialised at the first of every month. The ACCESS-S2 hindcast  
238 set used in this study runs for the period 1981–2018. Ensemble members are created in  
239 the same manner as ACCESS-S1 members, however, due to computing cost limitations,  
240 only three members per forecast initialisation date were run for 279 days. Bigger  
241 ensembles were generated by aggregating several three-member ensembles initialised  
242 on successive days<sup>16</sup>. Here, we build a nine-member time-lagged ensemble from three  
243 consecutive three-member forecasts initialised at the first of every month and the two  
244 previous days and run for 279 days. We analyse the ensemble mean hindcasts unless  
245 otherwise specified.

246  
247 Anomalies for each hindcast set are taken with respect to their own climatology specific  
248 to each initialisation date and forecast lead time, for the period 1990–2012. This serves  
249 as a first-order correction of model bias and drift. For monthly means, we define “0  
250 lead time months” as the monthly mean forecast of the same month of initialisation.  
251  
252 Besides sea-ice concentration, we also analyse mean sea-ice thickness, which we compute  
253 as total sea-ice volume divided by total sea-ice area.

254

255

## 256 **Verification datasets**

257

258 For verification we use satellite-derived sea-ice concentration, which estimates the  
259 proportion of each grid area that is covered with ice. Datasets derived using different  
260 algorithms and satellite platforms, each have their own biases and uncertainties.  
261 Estimates of inter-product uncertainty of sea-ice extent (SIE, defined here as the total  
262 region of the Southern Ocean with at least 15% sea-ice cover) are of the order of 0.5  
263  
264

million  $km^2$ <sup>29</sup>. As will be shown below, this spread is minimal compared with the typical errors in the ACCESS-S2 and ACCESS-S1 forecasts, so the overall conclusions of this study are independent of the verification dataset used.

We use NOAA/NSIDC's Climate Data Record V4 [CDR; Meier et al.<sup>30</sup>] as the primary sea-ice verification dataset. It takes the maximum value of the NASA Team<sup>31</sup> and NASA Bootstrap<sup>32</sup> sea-ice concentration products to reduce their low concentration bias<sup>30;33</sup>. Both source algorithms use data from the Scanning Multichannel Microwave Radiometer (SMMR) on the Nimbus-7 satellite and from the Special Sensor Microwave/Imager (SSM/I) sensors on the Defense Meteorological Satellite Program's (DMSP) -F8, -F11, and -F13 satellites. The data have a spatial resolution of 25 by 25 km and daily from November 1978 onwards.

The European Organisation for the Exploitation of Meteorological Satellites (EUMETSAT) Ocean and Sea Ice Satellite Application Facility [OSI; EUMETSAT Ocean and Sea Ice Satellite Application Facility<sup>34</sup>] based on the SSMIS sensor is another satellite-derived sea-ice concentration product. It is based on mostly the same sensors as the NOAA CDR but computed independently using different algorithms. Figures prepared with this dataset are provided in the supplementary material and do not differ significantly from the ones prepared using CDR.

## Error measures

For evaluation purposes, we use a series of measures. Sea-ice extent is defined as the area of the ocean at least 15% covered by sea-ice. This threshold is motivated by the limitations in satellite retrieval, which is increasingly unreliable for lower sea-ice concentrations<sup>35</sup>.

Pan-Antarctic (net) sea-ice extent serves as a hemispheric measure of the amount of sea ice, but it does not take into account the spatial distribution. A model could have

323 a relatively accurate extent of the net ice but with different regional distributions. To  
 324 account for location errors, we computed the Root Mean Squared Error (RMSE) of  
 325 grid-point sea-ice concentration anomalies.  
 326  
 327 We compute RMSE as the square root of the area-averaged squared differences between  
 328 grid-point forecasted and observed sea-ice concentration anomalies. We compute a  
 329 pan-Antarctic RMSE by averaging over the whole NOAA/NSIDC CDRV4 Southern  
 330 Hemisphere domain, and also a zonally-varying RMSE computed over 15 longitude  
 331 slices  $24^{\circ}$  wide around Antarctica.  
 332  
 333 All error measures were computed on the NOAA/NSIDC CDRV4 domain grid, to  
 334 which model output was bilinearly interpolated. Note that the ACCESS CICE model  
 335 grid has resolution between two and three times higher than NOAA/NSIDC CDRV4.  
 336  
 337 Forecast errors are also compared with hypothetical forecasts based on the persistence  
 338 of anomalies and on climatology. The persistence forecast is generated by extending  
 339 the observed sea-ice concentration anomalies the day of the forecast initialisation and  
 340 comparing it with the actual anomalies observed. The climatological forecast error is  
 341 computed as the standard deviation of daily anomalies.  
 342  
 343 As a measure of forecast improvement over the hypothetical forecast, we use the skill  
 344 score<sup>36</sup>, defined as  
 345  
 346
 
$$S = 1 - \frac{RMSE_f}{RMSE_r}$$
 347  
 348 Where  $RMSE_f$  is the RMSE of the forecast,  $RMSE_r$  is the RMSE of the reference  
 349 forecast. Negative skill score indicates that the forecast is worse than the reference  
 350 forecast while positive values indicate an improvement. A perfect forecast would have  
 351 zero RMSE and thus a skill score of 1.  
 352  
 353

## Computational procedures

369

370

371

372

373

374

375

376

377

378

379

380

381

382

383

384

385

386

387

388

389

390

391

392

393

394

395

396

397

398

399

400

401

402

403

404

405

406

407

408

409

410

411

412

413

414

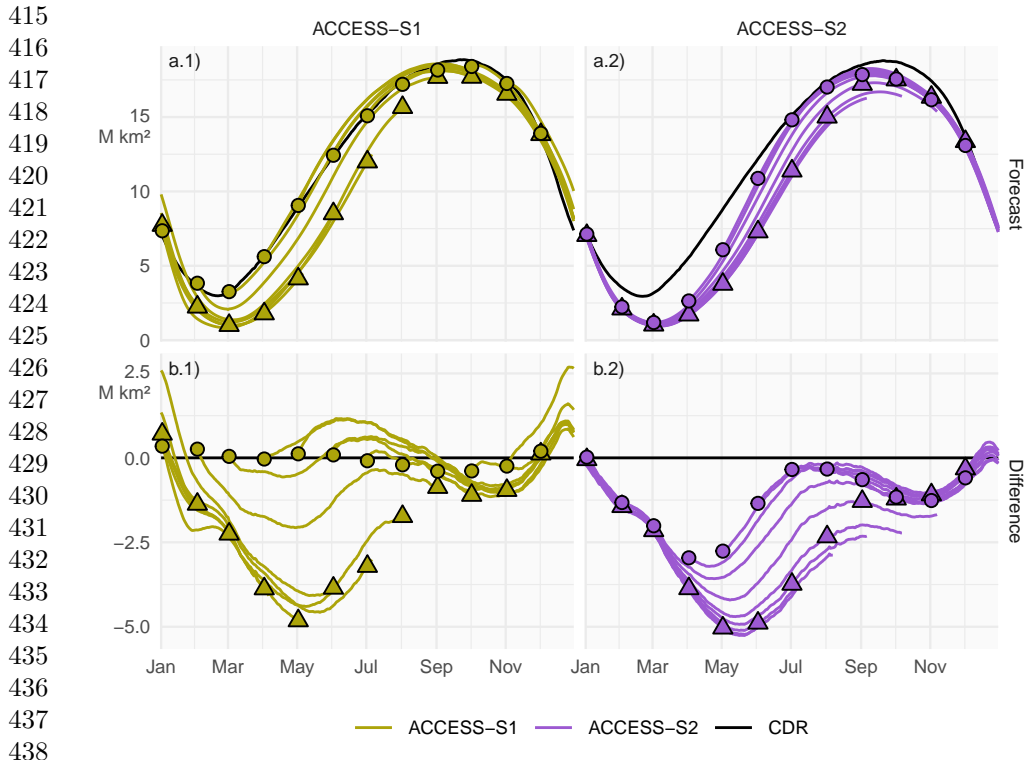
We performed all analyses in this paper using the R programming language<sup>37</sup>, using data.table<sup>38</sup> and metR<sup>39</sup> packages. Significant processing was performed using the CDO command line operators<sup>40</sup>. All graphics are made using ggplot2<sup>41</sup>. The paper was rendered using knitr and Quarto<sup>42;43</sup>.

## Results and discussion

### Bias

Figure 1 shows mean sea-ice extent of the ACCESS-S1 and ACCESS-S2 hindcasts (row a) and their differences from mean sea-ice extent of NOAA/NSIDC CDRV4 (row b). Mean extent at the first of every month is indicated with circles for the initial conditions and with triangles for the longest lead time possible for each model (between 274 and 277 days for ACCESS-S2 and between 213 and 216 days for ACCESS-S1). At this long lead time, information of the initial conditions is essentially lost and the forecast reverts close to each model's preferred equilibrium state.

ACCESS-S2 initial conditions (circles in Fig. 1 column 2) show an overall negative bias, especially in the late summer-early autumn, while ACCESS-S1 initial conditions (circles in Fig. 1 column 1) are very close to observations, as expected from the assimilation of sea-ice observations to produce the initial conditions of ACCESS-S1. Both systems' equilibrium states (triangles) show negative biases of sea-ice extent, particularly in the growth phase of late-autumn and winter months. This is due primarily to the melt season being longer than in observations and with faster melt between January and March and the growing seasons being shorter with slower growth during March and April. This is then followed by faster growth between May and July (Figure 2). Many sea-ice models exhibit this systematic underestimation during the sea-ice minimum



439 **Figure 1:** Row a: Pan-Antarctic daily mean sea-ice extent for all hindcasts initialised  
440 on the first of each calendar month for ACCESS-S1 (column 1; green) and ACCESS-S2  
441 (column 2; purple). Observed mean sea-ice extent in each corresponding hindcast period  
442 is shown in black. Row b: Mean differences between the forecast and the observed  
443 values. Circles represent the initial conditions at the start of forecasts (i.e., the first of  
444 every month), and triangles represent the mean values at the lead time corresponding  
445 to the maximum lead time in S1 (between 213 and 216 days, depending on the month)  
446  
447

448 and early freezing season<sup>8</sup>, which could indicate problems in the representation of  
449 thermodynamics in the model<sup>6</sup>. It is also not surprising that both forecasting systems  
450 converge to a similar equilibrium state because they share the same model formulation.  
451  
452 The difference between the initial conditions (circles) and the model equilibrium  
453 state (triangles) can be mostly attributed to the effect of data assimilation, which  
454 in ACCESS-S2 is due solely to the coupling of sea-ice with the atmosphere and the  
455 ocean. From May to October, in ACCESS-S2 circles are closer to observations than  
456  
457  
458  
459  
460

the triangles are, indicating that the information from the ocean and atmosphere data assimilation is affecting sea ice and improving the initial conditions. During these months, ACCESS-S1 can overestimate the sea-ice extent at short lead time. For the rest of the year circles are overlaid with triangles in ACCESS-S2, indicating that the ocean and atmosphere data assimilation is not affecting sea ice and that this component of the model is virtually free-running.

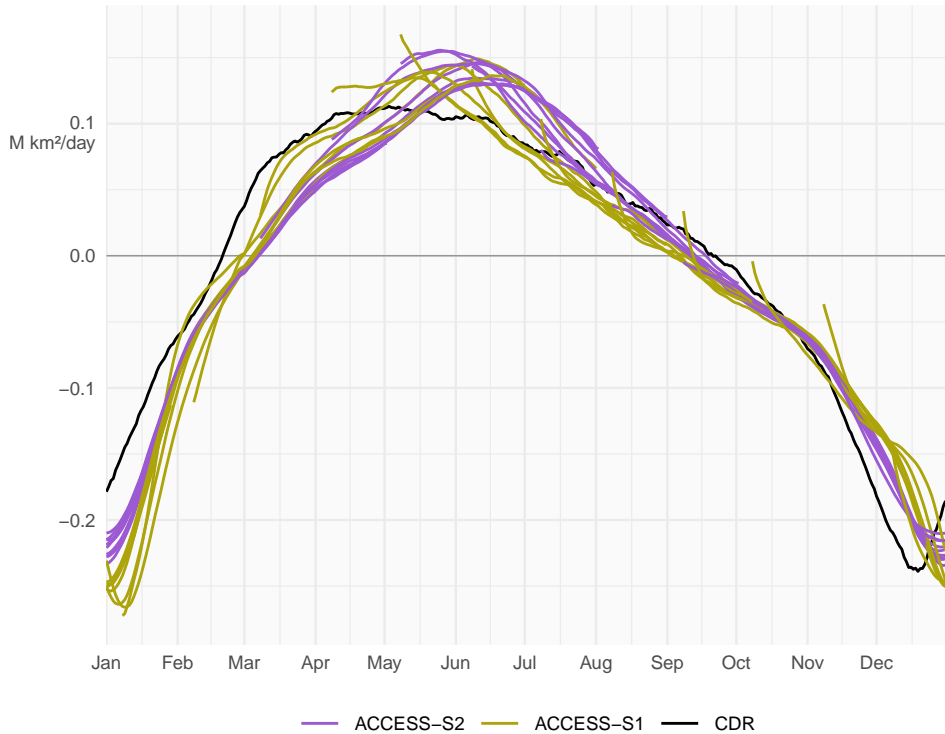
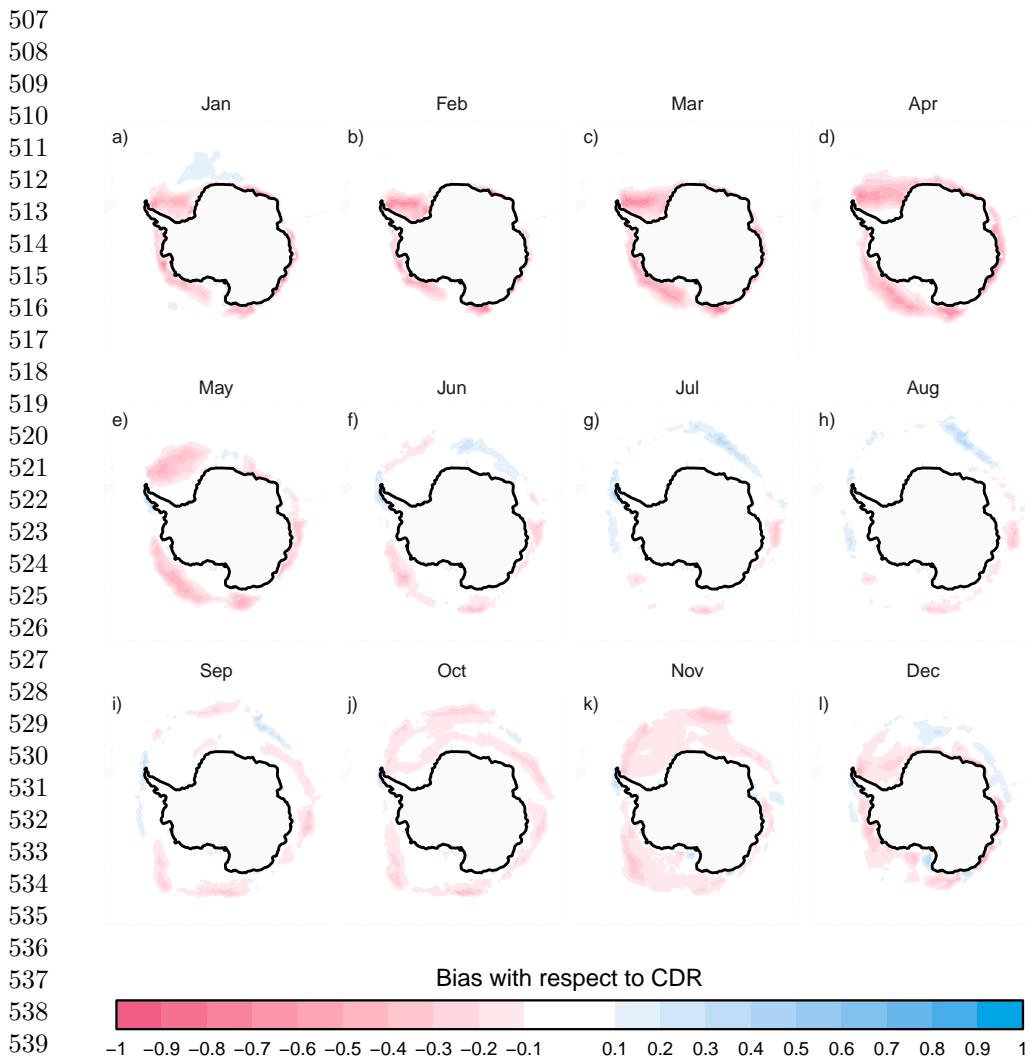


**Figure 2:** Mean daily sea-ice extent growth ( $10^6 \text{ km}^2/\text{day}$ ) in ACCESS-S1 (green) and ACCESS-S2 (purple) hindcasts and observations (black), computed as the mean daily differences in sea-ice extent between each date and the next for each forecast month. Values are smoothed with a 11-day running mean.

To further understand the bias in ACCESS-S2, Figure 3 shows spatial patterns of the differences of monthly mean sea-ice concentrations between NOAA/NSIDC CDRV4 and ACCESS-S2 hindcasts at the shortest monthly lead time. From October to May,



543 **Figure 3:** Ensemble mean difference between monthly sea-ice concentration of  
 544 ACCESS-S2 ensemble mean forecast at 0-month lead time (monthly mean values fore-  
 545 casted from the forecast initialised at the first of the month) and observations (CDR).

546  
 547  
 548 the model underestimates sea-ice concentrations in most regions except for the inner  
 549 Weddell Sea in April and May, where sea-ice concentrations saturate to 1 both in  
 550 the observations and forecasts. In winter, the differences are limited to a narrow  
 551  
 552

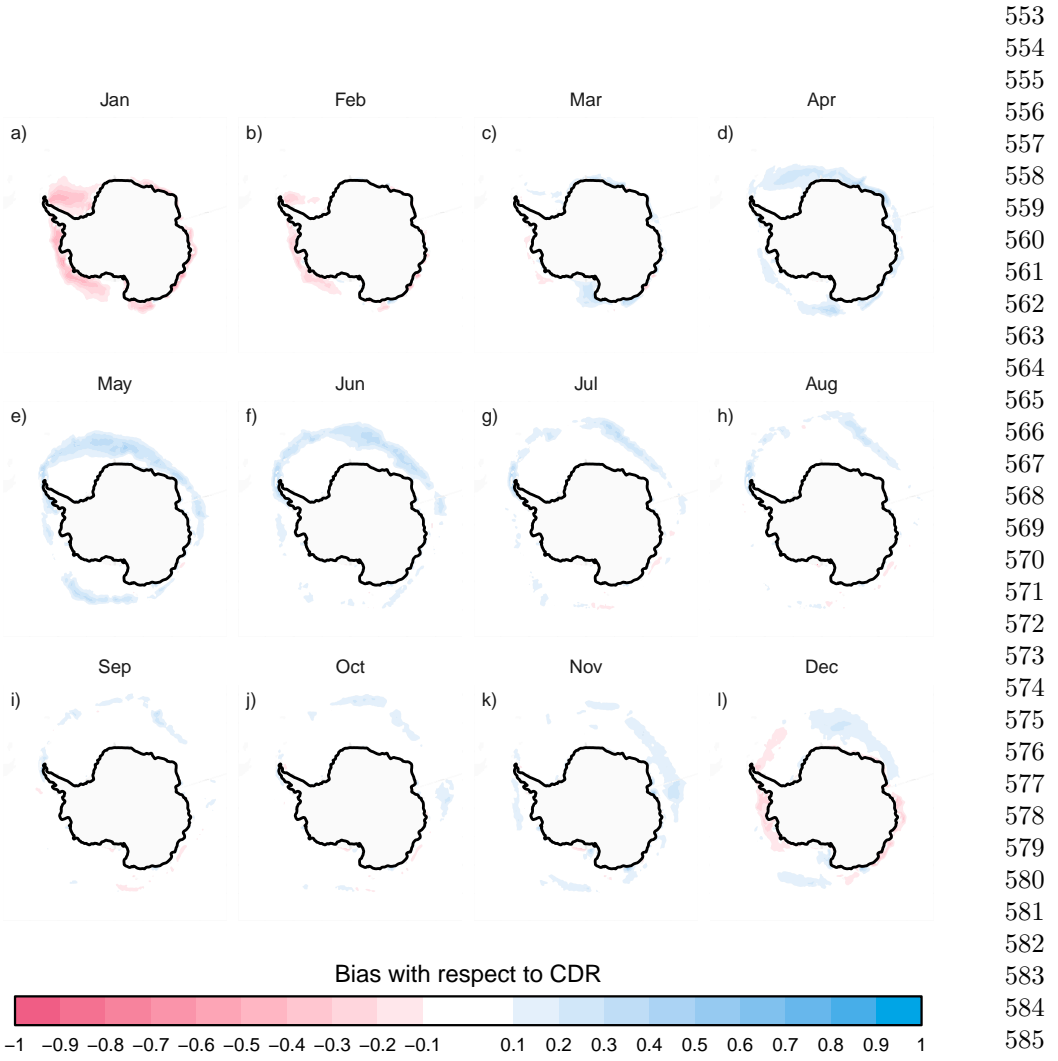


**Figure 4:** Same as Figure 3 but for ACCESS-S1.

band around the sea-ice edge with slight positive biases in the African sector of East Antarctica and negative biases around the Indian Ocean sector which partially compensate, resulting in the near-zero extent bias seen in those months (Figure 1).

599 ACCESS-S1 has a comparatively smaller overall bias (Figure 4). The largest values are  
600 found between April and June, when the faster growth results in large positive bias  
601 along the sea-ice edge, and in January, when the faster melt leads to large negative  
602 bias in the Weddell and Amundsen Seas.  
603

604

605

606

## 607 RMSE

608

609

610 Figure 5 shows monthly sea-ice extent anomalies forecasted at selected lead times.  
611 Compared with ACCESS-S1, ACCESS-S2 anomaly forecasts are relatively poor (large  
612 RMSE) even for the first month (lead time 0), whereas ACCESS-S1 forecasts stay  
613 relatively skilful even at a lead time of three months. ACCESS-S2 shows much larger  
614 interannual variability than observations, with dramatic lows between 1995 and 2007,  
615 and highs between 2007 and 2015.  
616

617

618 Unexpectedly, for ACCESS-S2, RMSE improves with lead time, even though the cor-  
619 relation degrades with lead time. This is puzzling behaviour that goes contrary to  
620 what is usually seen in prediction models. The explanation seems to be the mentioned  
621 increased interannual variability. Figure 6 shows the interannual standard deviation  
622 of monthly sea-ice extent of the forecasts as a function of lead time compared with  
623 observations. ACCESS-S1 standard deviation lies within the observed standard devia-  
624 tion regardless of lead time, while ACCESS-S2 standard deviation is more than twice  
625 that of observations at zero lead time and only approaches the observed value at nine  
626 months lead time for most months.  
627

628

629 ACCESS-S2 forecasts of sea-ice extent anomalies seem to align moderately well with  
630 observations (leading to moderately high correlation) but their magnitude is overesti-  
631 mated (leading to large errors). This could be caused by ACCESS-S2 sea ice being much  
632 more sensitive to atmospheric and oceanic forcing, perhaps due to lower thickness.  
633

634

635

636

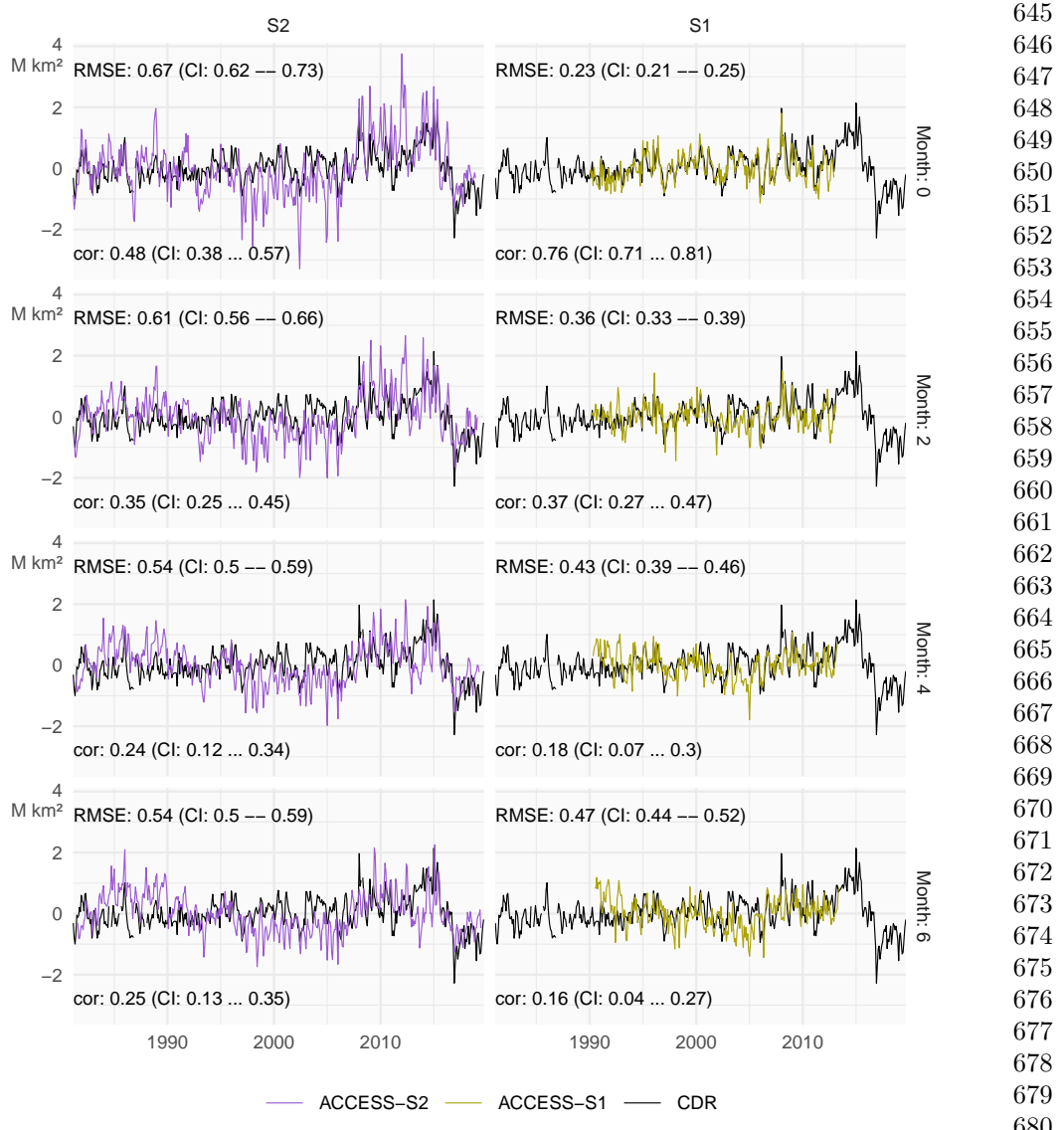
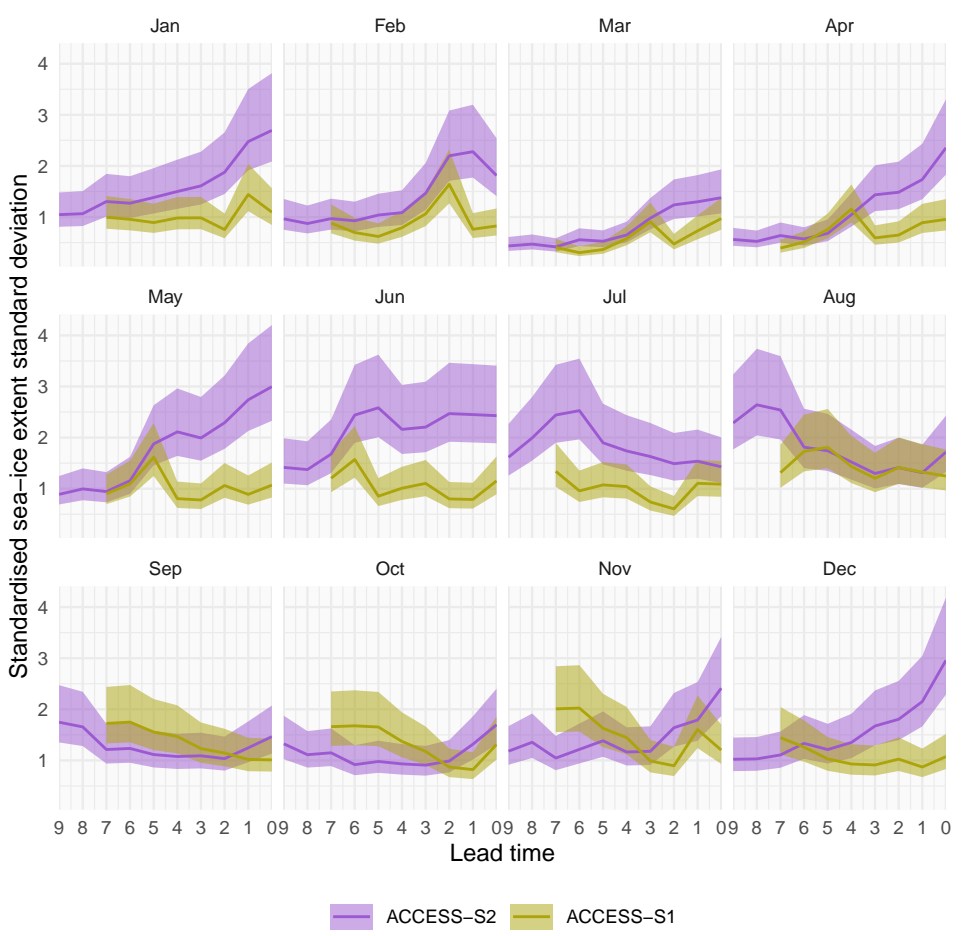


**Figure 5:** Monthly mean sea-ice extent anomalies of the observations (black) and forecasts from ACCESS-S1 (right column; purple) and ACCESS-S2 (left column; green) at lead times of 0, 2, 4, and 6 months. The RMSE and correlation during the overlapping period of ACCESS-S1 and ACCESS-S2 hindcasts (1990–2013) are shown on the top left and bottom left of each panel respectively.

As an example, Figure 7 shows sea-ice concentration anomalies (top row) and sea-ice thickness and the difference between the two models (bottom row) for 2 May



721 **Figure 6:** Interannual standard deviation with 95% confidence interval of monthly  
 722 mean sea-ice extent forecasted for each month divided by that month's sea-ice extent  
 723 observation standard deviation. ACCESS-S1 and ACCESS-S2 at different lead times.  
 724 Each panel indicates the target month. Note the reverse horizontal axis.

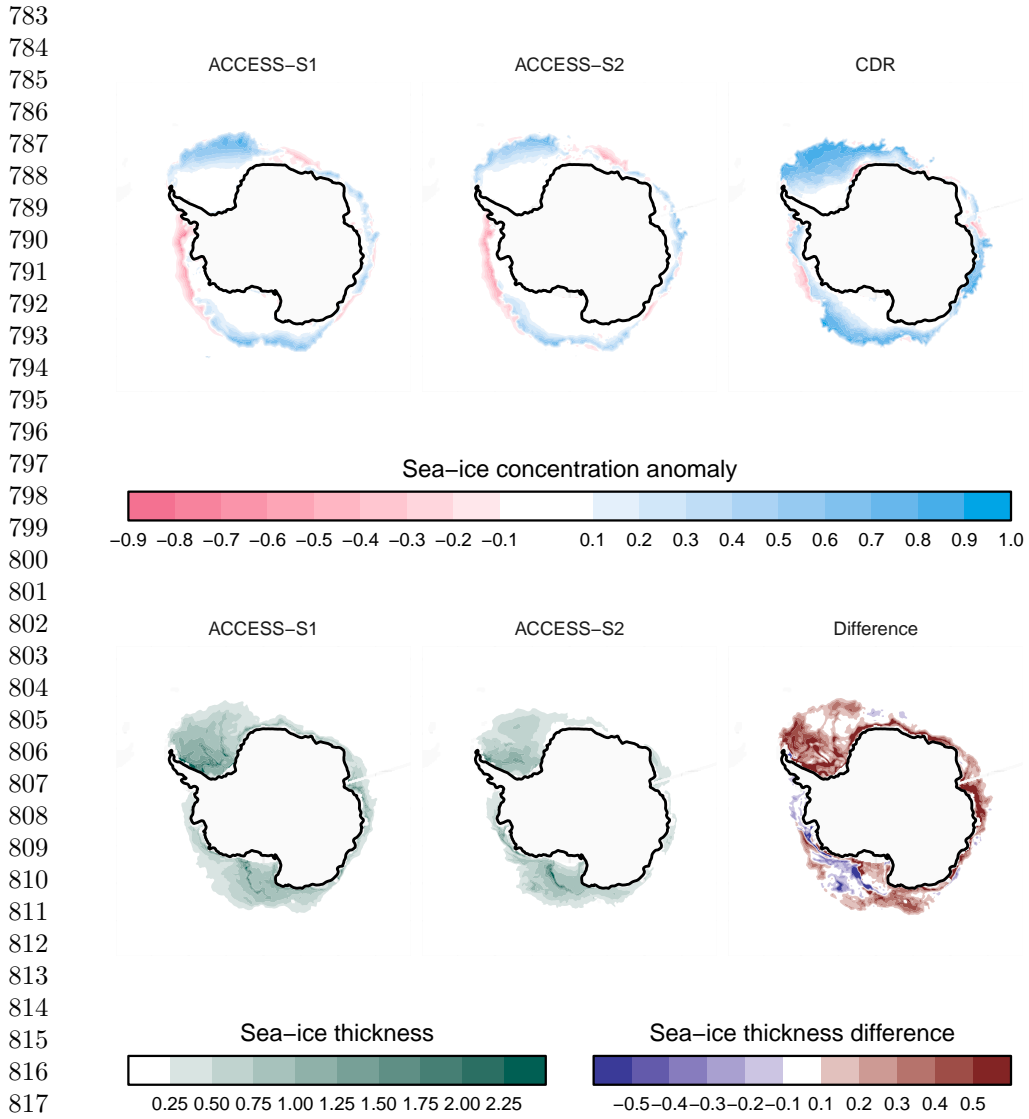
725  
 726  
 727 2008 initialised one day prior; being that close to initialisation date, these are very  
 728 approximately the initial conditions. ACCESS-S1 sea-ice concentrations anomalies  
 729 are very close to observations as expected from the system assimilating these data.  
 730  
 731 ACCESS-S2 sea-ice concentration anomalies, which are not assimilated, are not as  
 732 close, but the large-scale pattern is aligned with observations. The system simulates  
 733  
 734 large positive anomalies in the Weddell and Ross Seas and slight negative anomalies  
 735  
 736

in the Amundsen and Bellingshausen Seas. The fact that ACCESS-S2 can simulate  
this pattern without assimilating sea-ice data suggests that atmospheric and oceanic  
forcing were the dominant drivers. However, the magnitude of the sea-ice anomalies is  
too big. It is plausible that this is due to the thinner ice simulated by ACCESS-S2  
(bottom row).

Extending beyond the one case in Figure 7, Figure 8 shows monthly mean sea-ice  
thickness as a function of lead time for ACCESS-S1 and ACCESS-S2. Supporting the  
idea that thinner ice is what causes the increased extent variability in ACCESS-S2,  
this system simulates thinner sea-ice compared to ACCESS-S1 overall at almost all  
lead times and in all months except for summer at short lead times (Dec-Jan, 0-1  
months; Feb-Mar, 0-2 months). However, in both systems, forecasted sea-ice is thicker  
at shorter lead times and then decreases, particularly in the summer months. If thinner  
ice were a sufficient cause of increased variability, then we would expect variability to  
increase with lead time in both forecasting systems.

The fact that ACCESS-S1 and ACCESS-S2 share the same model configuration and  
that the increased variability is more extreme at short lead times (Fig. 6) suggests  
that the data assimilation procedure is partly responsible. It is possible that sea-ice in  
the ACCESS-S2 system is left in an unbalanced state after assimilating atmospheric  
and oceanic data but not sea-ice data, leading to large responses that are amplified  
by the thin ice in the initial states which then subside at longer lead times when the  
model is balanced.

To assess ACCESS-S2 forecasts in more detail, we compute error measures for all  
hindcasts started on the 1st of every month. Figure 9 shows the mean RMSE of sea-ice  
concentration anomalies for ACCESS-S1 and ACCESS-S2 hindcasts compared against  
persistence and climatological forecasts used as a benchmark. Due to errors in the  
initial conditions, it is expected that persistence forecasts would be better than the  
model forecasts at very short lead times, but that the persistence forecast errors would



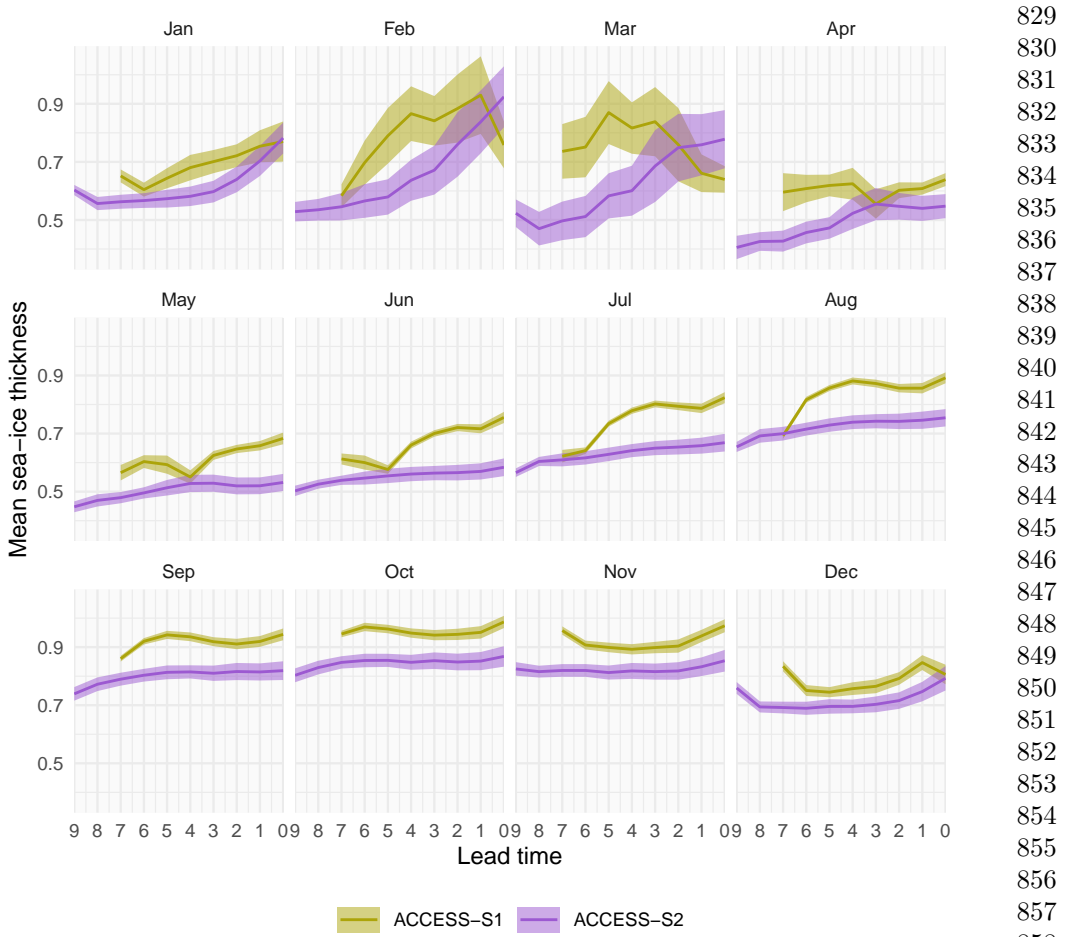
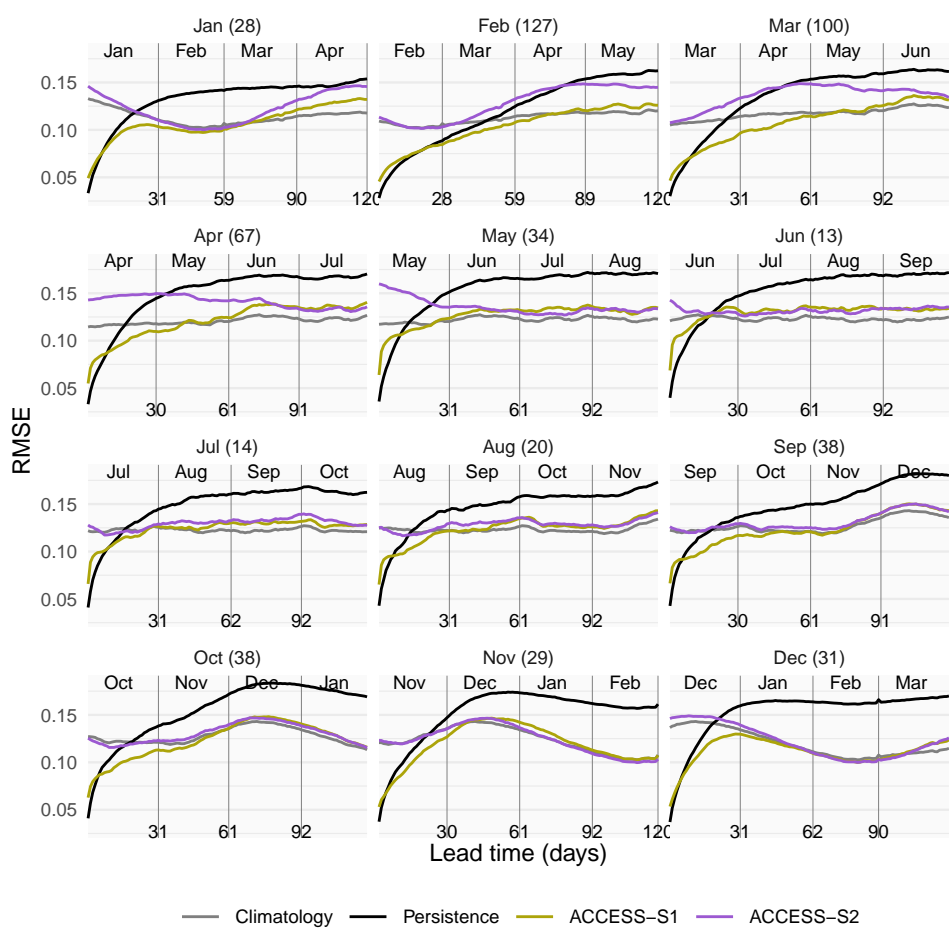


**Figure 8:** Mean and 95% interval of monthly mean sea-ice thickness for ACCESS-S1 and ACCESS-S2 at different lead times. Each panel indicates the target month. Note the reverse horizontal axis.

about 30 days for most months except for February, when it grows much slower. The ACCESS-S1 forecast errors grow slower than persistence forecast errors and remain lower after less than 10 days on average. The ACCESS-S2 forecast error starts high in all months and is lower than the persistence forecast error after more than 15 days in most months except for forecast initialised in February, when it takes 80 days.



905 **Figure 9:** Mean RMSE of sea-ice concentration anomalies as a function of forecast  
906 lead time for all forecasts initialised on the first of each month compared with a  
907 reference forecast of persistence of anomalies (black) and climatology (gray). Only the  
908 first 120 days are shown. In parentheses, the shortest time at which ACCESS-S1 and  
909 ACCESS-S2 mean RMSE is not statistically different at the 99% confidence level.

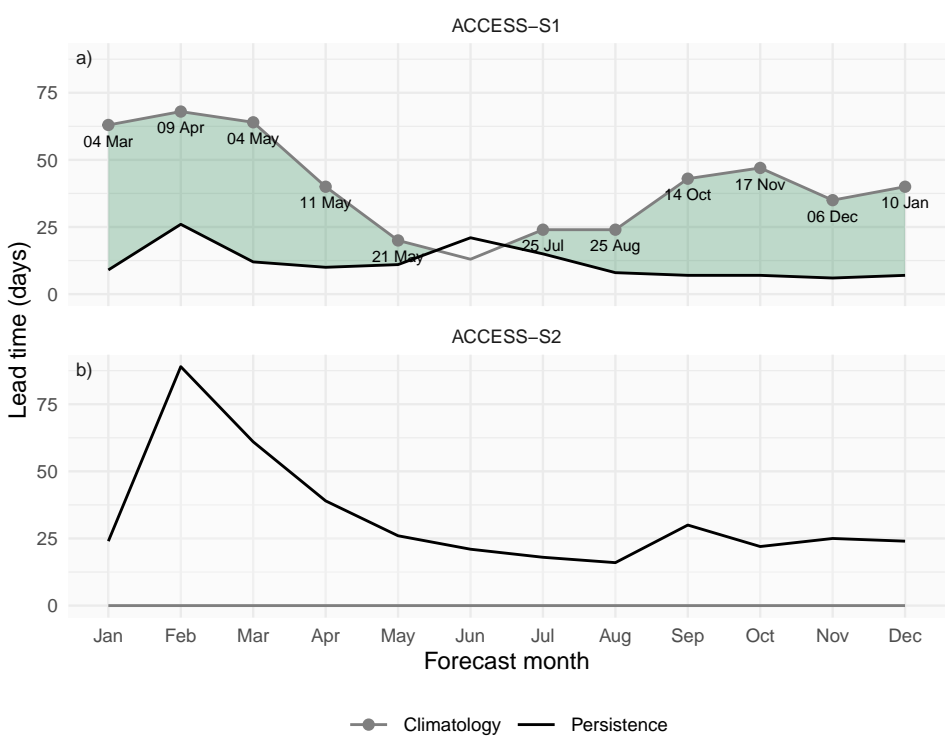
910  
911  
912 At longer lead times, it is more appropriate to compare errors with the climatological  
913 forecast error. The lead time at which ACCESS-S1 forecast error is higher than  
914 the climatological forecast error varies between more than 60 and less than 20 days  
915 depending on forecast initialisation month with the minimum in June. ACCESS-S2  
916  
917  
918  
919  
920

forecasts never have lower error than climatology, on the other hand, except marginally  
in October forecasts. 921  
922  
923

Figure 10 summarises the lead time window in which each hindcast is better than  
both the persistence forecast and the climatological forecast as a function of forecast  
month. ACCESS-S1 forecasts have a wider lead time window in the summer than  
the other seasons and is not better than both benchmarks at forecasting June sea-ice  
concentration anomalies. Forecasts initialised in May and June are particularly poor,  
and July cannot be forecasted better than the benchmarks. This is consistent with  
the mid-winter loss of predictability observed by Libera et al.<sup>44</sup>, who attributed it to  
deep warm water entraining into the mixed layer. 924  
925  
926  
927  
928  
929  
930  
931  
932  
933  
934  
935  
936  
937  
938  
939  
940  
941  
942  
943  
944  
945  
946  
947  
948  
949  
950  
951  
952  
953  
954  
955  
956  
957  
958  
959  
960  
961  
962  
963  
964  
965  
966

To analyse the spatial distribution of the model error, we computed the RMSE of  
zonal mean sea-ice concentration anomalies on 15 slices of 24° longitude span for each  
forecasting system. We control for some areas being naturally easier to forecast than  
others by computing the RMSE skill score with the climatological forecast RMSE as  
reference. 938  
939  
940  
941  
942  
943  
944  
945  
946  
947  
948  
949  
950  
951  
952  
953  
954  
955  
956  
957  
958  
959  
960  
961  
962  
963  
964  
965  
966

For ACCESS-S1 forecasts (Figure 11), skill tends to be lower off the coast of Eastern  
Antarctica even at short lead times; for instance, the skill score for forecasts initialised  
in May and June are negative between 0° and 120°E even at almost zero lead time.  
This mirrors Libera et al.<sup>44</sup> findings of a “winter predictability barrier”, although they  
focus on the Weddell Sea and here we show that the effect seems to be stronger more  
to the east. In West Antarctica there is a hint of easterly-propagating skill in forecasts  
initialised in February and March. This is consistent with Holland et al.<sup>13</sup> findings  
that memory of sea-ice anomalies are stored in ocean heat content anomalies that are  
transported east by the Antarctic Circumpolar Current. 947  
948  
949  
950  
951  
952  
953  
954  
955  
956  
957  
958  
959  
960  
961  
962  
963  
964  
965  
966



991 **Figure 10:** Minimum lead time at which each forecast's mean RMSE becomes larger  
992 than the lower bound of the 95% confidence interval of persistence forecast RMSE  
993 (black lines) and maximum lead time at which each forecast's mean RMSE remains  
994 lower than the lower bound of the 95% confidence interval of climatological forecast  
995 RMSE (gray lines). Green shading indicates the window where forecasts outperform  
996 both persistence (lead times longer than black line) and climatology (lead times shorter  
997 than gray line). Text labels show the date corresponding to the maximum lead time at  
998 which each forecast outperforms climatology.  
999  
1000

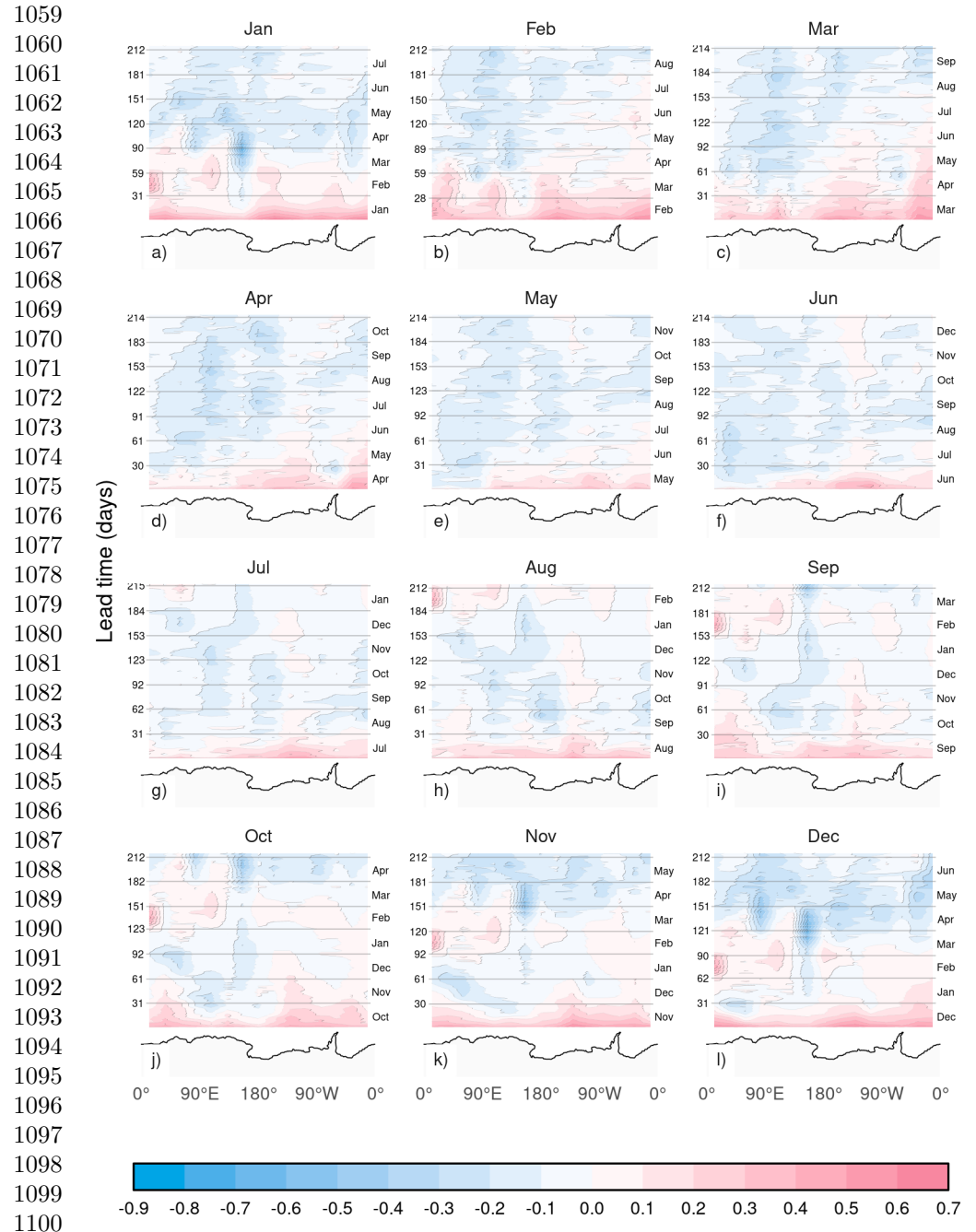
1001 times (Fig. 10), it is positive for up to a month in West Antarctica. Since oceanic and  
1002 atmospheric forcing is the only source of information, this suggests that sea-ice in  
1003 this region is particularly sensitive to oceanic and atmospheric forcing and suggests a  
1004 role of the Pacific-South American mode and the Amundsen Sea Low to shape sea-ice  
1005 concentration anomalies. The fact that this is evident in the months in which El Niño–  
1006 Southern Oscillation teleconnections are more important for atmospheric circulation  
1007  
1008  
1009  
1010  
1011  
1012

also suggests the influence of tropical Pacific variability. February and March are the  
only two months that can be forecasted with marginally positive skill in large regions.

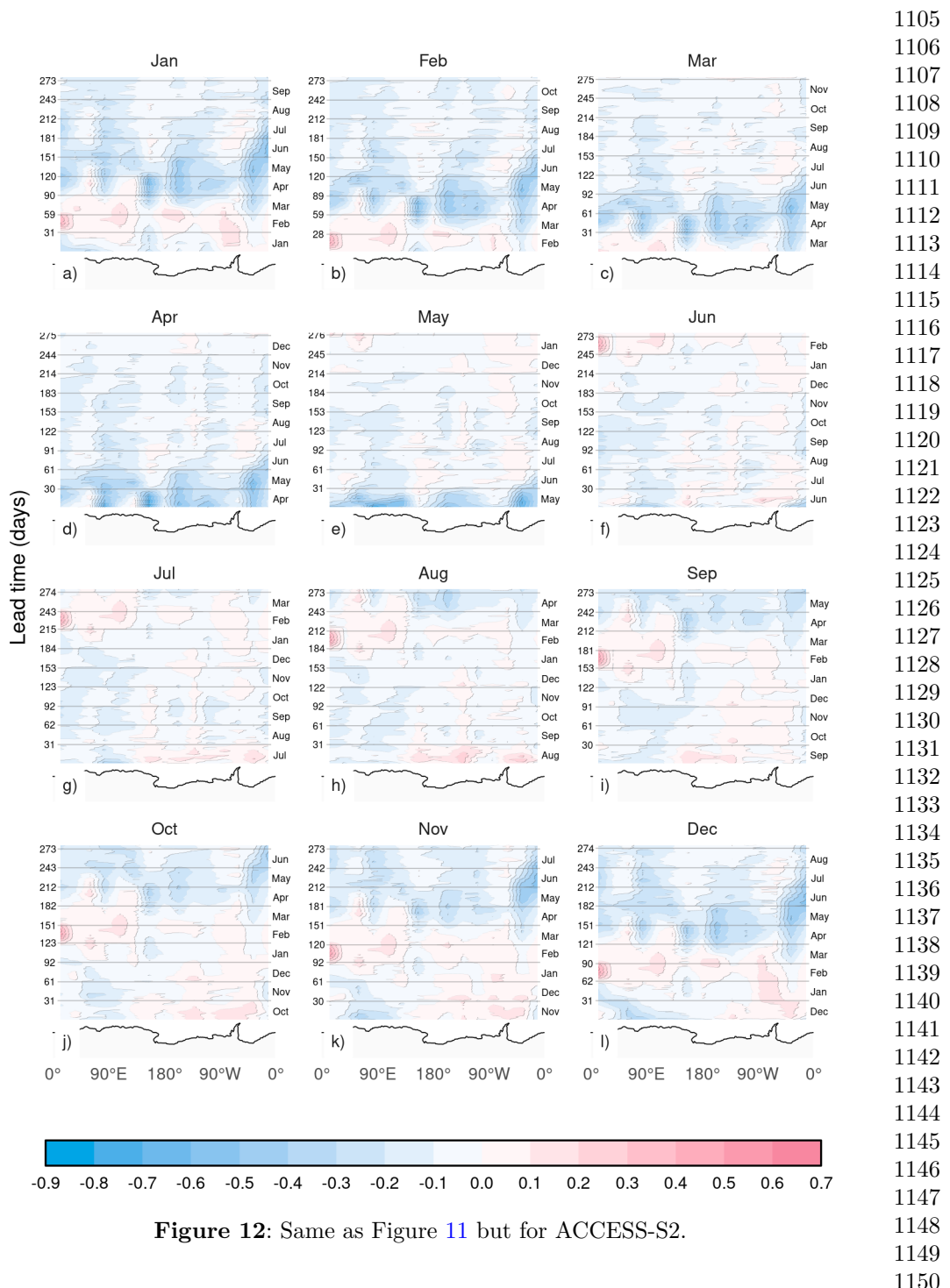
Finally, Figure 13 shows the difference in skill between ACCESS-S1 and ACCESS-S2.  
Large differences in skill indicate areas and months that are most affected by the  
data assimilation present in ACCESS-S1. Between January and March, which are the  
months in which ACCESS-S1 is the most skilful (Figure 10), most of the improvement  
compared with ACCESS-S2 is present in the Ross and Weddell Sea. In April and May,  
the improvement seems more homogeneous.

In Figure 9 the mean error was shown. Figure 14 column 1 shows the mean standard  
deviation of errors among ensemble members at various lead times. At one day lead  
time (Fig. 14 a.1) ACCESS-S2 has a slightly larger spread than ACCESS-S1 due  
to the way that ensemble members are generated. ACCESS-S1 ensemble members  
are generated by adding random field perturbations to the atmosphere only, which  
then are transferred to the other components via the coupled simulation<sup>17</sup>. With this  
scheme, ensemble members are all but guaranteed to be underdispersed in the ocean  
and sea-ice components. The time-lag ensemble used for ACCESS-S2 ensures greater  
spread. This difference is gone after about just two days, and both systems have a  
comparable spread in ensemble member error afterwards (Fig. 14 b1 and c1).

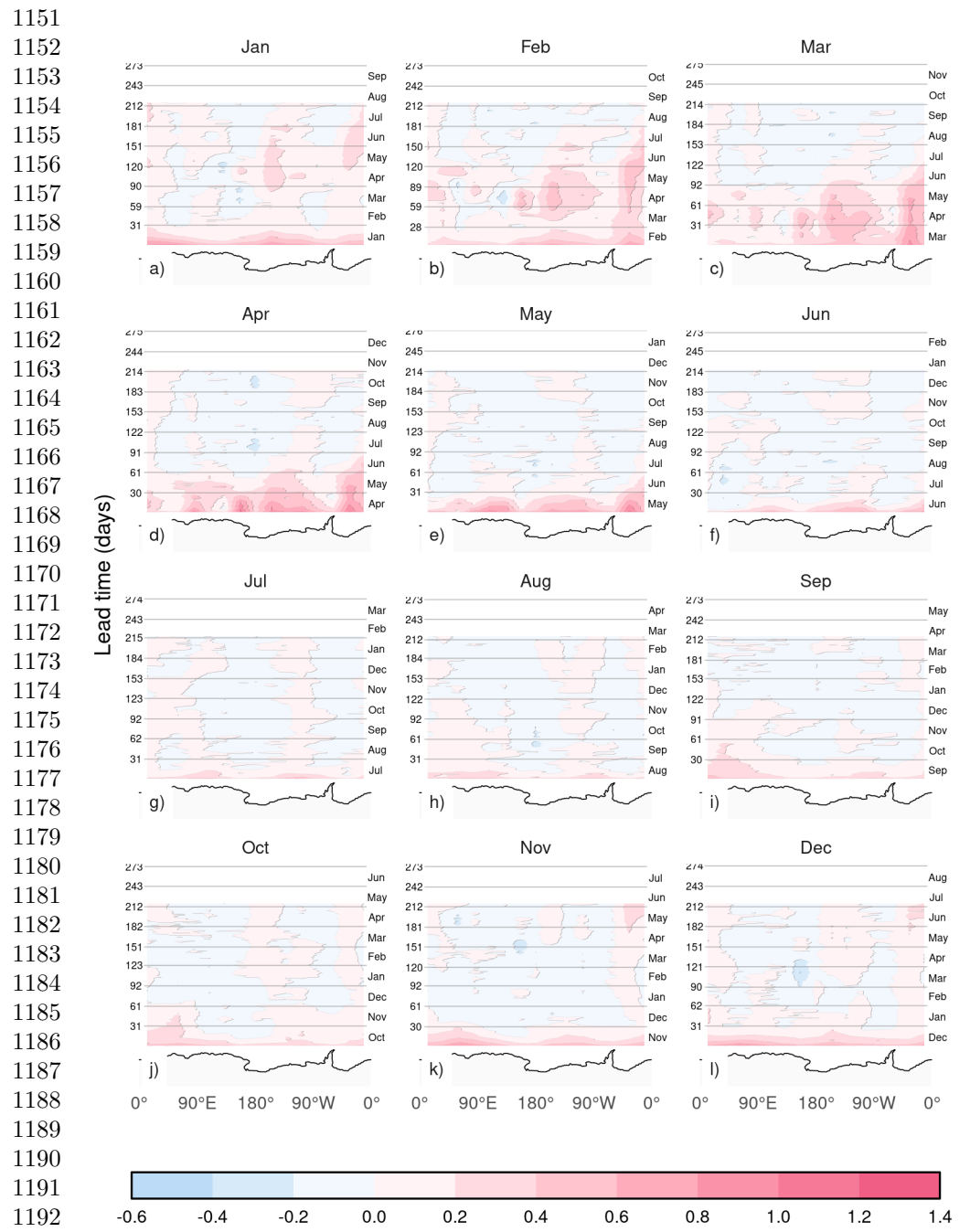
Figure 14 column 2, on the other hand, shows the standard deviation of ensemble mean  
error of each hindcast and the persistence forecast. At one day lead time, ACCESS-S2  
ensemble mean error standard deviation is much larger than ACCESS-S1's, which in  
turn is comparable to the persistence forecast error standard deviation. At longer lead  
times, the spread of ACCESS-S1 and persistence forecast standard deviation increases  
to eventually be comparable to ACCESS-S2 and the standard deviation in climatological  
forecast errors. ACCESS-S2 error standard deviation is fairly independent of lead time  
and similar to the climatological forecast error standard deviation at all lead times.



1101 **Figure 11:** RMSE skill score of ACCESS-S1 forecasts with climatological forecast as  
 1102 reference computed on 15 meridional slices  $24^\circ$  wide as a function of lead time and  
 1103 longitude. Antarctica's coastline is shown at the bottom of each panel for reference.  
 1104



**Figure 12:** Same as Figure 11 but for ACCESS-S2.



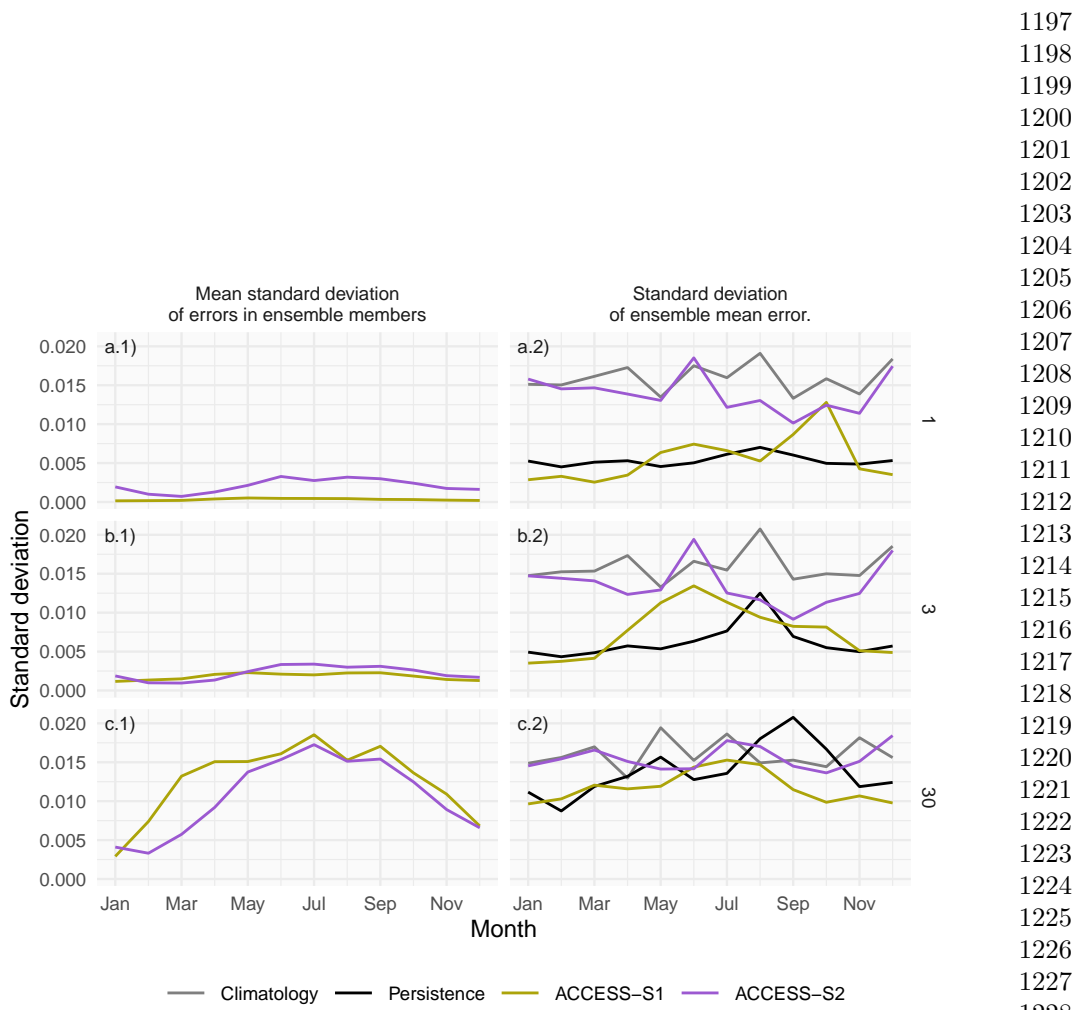


**Figure 14:** Decomposition of forecast error spread at 1, 5 and 30 days lead time for ACCESS-S1 and ACCESS-S2 hindcasts across initialization months. The left column shows the mean standard deviation of RMSE errors across ensemble members, while the right column shows the standard deviation of the ensemble mean RMSE error and the spread of the persistence and climatology forecasts errors.

1243 **Conclusions**

1244

1245

1246 Sea-ice forecasts from the ACCESS-S2 system show a significant low extent bias,  
1247 particularly during late summer and early autumn. This bias is attributed to a faster  
1248  
1249 and longer melt season between January and March, and slower growth between March  
1250  
1251 and April. This underestimation during the minimum and early freezing season is a  
1252 common issue in many seasonal-to-subseasonal (S2S) systems, suggesting potential  
1253  
1254 problems either with the model's thermodynamic representation or with short wave  
1255  
1256 radiation forcing, as shown in other climate models<sup>6;45</sup>. Even though ACCESS-S2  
1257 shares the same model components as ACCESS-S1, the latter does not suffer from  
1258  
1259 this bias, indicating that assimilating sea-ice concentrations successfully corrects for  
1260  
1261 the negative bias that exists in the free-running model.

1262

1263 Ensemble spread grows quickly even when perturbations are only implemented in the  
1264 atmosphere component (in ACCESS-S1), indicating that sea ice is indeed responding  
1265  
1266 quickly to atmospheric perturbations. However, our analysis suggests that the atmo-  
1267  
1268 sphere and ocean data assimilation implemented in ACCESS-S2 is only effectively  
1269 influencing sea-ice initial conditions from June to October, while the rest of the year,  
1270  
1271 the sea-ice component runs virtually free, reverting to its biased equilibrium state.  
1272

1273 Zhou and Alves<sup>46</sup> had previously evaluated sea-ice forecasts in ACCESS-S2 and also  
1274 highlighted the poor performance of this forecasting system attributed to the lack of  
1275  
1276 good initial conditions.

1277

1278 Analysis of the error spread shows that ACCESS-S2 initial conditions from December  
1279  
1280 to May not only have large errors, but that the initial error spread is very large  
1281  
1282 compared with ACCESS-S1. This spread is not due to the perturbation scheme, since  
1283  
1284 the mean error variance for individual forecasts is low and comparable with ACCESS-  
1285 S1. Instead, it is due to large variance of the mean error of individual forecasts, which  
1286  
1287

1288

is comparable to the climatology spread. This is further evidence that individual initial conditions are not being affected by the data assimilation scheme. 1289  
1290  
1291  
1292  
1293  
1294  
1295  
1296  
1297  
1298  
1299  
1300  
1301  
1302  
1303  
1304  
1305  
1306  
1307  
1308  
1309  
1310  
1311  
1312  
1313  
1314  
1315  
1316  
1317  
1318  
1319  
1320  
1321  
1322  
1323  
1324  
1325  
1326  
1327  
1328  
1329  
1330  
1331  
1332  
1333  
1334

Although ACCESS-S1 only assimilates sea-ice concentration, it is clear that sea-ice thickness is also affected through the assimilation process. ACCESS-S1 simulates significantly thicker ice than ACCESS-S2 and in both systems sea-ice is thicker at shorter lead times than at longer lead times. Both the explicit data assimilation in ACCESS-S2 and the effects of atmospheric and oceanic data assimilation in ACCESS-S1 might be nudging simulated sea ice to be thicker than the model equilibrium state. We suggest that the thinner sea ice in ACCESS-S2 contributes to the large sea-ice extent variance, but other mechanisms, such as unbalanced initial conditions might also be important.

Given that ACCESS-S2 sea-ice extent is not directly initialised by sea-ice observations, comparing its forecasts with those of ACCESS-S1 allows us to estimate the time-scale over which initial conditions are important. We find that initial conditions affect Antarctic sea-ice forecasts in the order of a few months, but that effect is seasonally dependent. January to April initial conditions improve forecasts for up to three months. February initial conditions in particular are shown to be crucial for determining sea-ice evolution at least up to May. Arctic sea-ice forecasts also show greater sensitivity to initial conditions in boreal summer, compared with boreal winter<sup>12;47</sup>, suggesting a similar mechanism might be playing a role.

Forecasts initialised in winter have very little skill and ACCESS-S1 and ACCESS-S2 forecast errors are statistically indistinguishable after just two weeks. This is consistent with Libera et al.<sup>44</sup>'s finding of a "winter predictability barrier" in the Weddell Sea, although they describe the barrier as a sharp loss of predictability in July, and here we find a gradual reduction in skill compared with climatology around June. This difference might be due to our use of pan-Antarctic RMSE, since our regional analysis indicates that the degraded skill is most dramatic in the King Haakon Sea.

1335 These findings have important implications for both operational forecasting, model  
1336 development and predictability studies. For operational centers, our results suggest that  
1337 efforts to improve sea-ice data assimilation should prioritize the summer and autumn  
1338 months when initial conditions have the greatest impact on forecast skill. Additionally,  
1339 the substantial bias in ACCESS-S2 highlights the need for improved model physics,  
1340 particularly in the representation of sea-ice thermodynamics and radiation processes.  
1341 Crucially, our results suggest dramatic seasonal variations in sea-ice predictability.  
1342 Future studies should therefore use initial conditions through the whole year rather  
1343 than focusing on a limited number of initialisation dates.  
1344

1350

1351

## 1352 **Acknowledgments**

1353

1354

1355 We thank the internal reviewers Bethan White and Xiaobing Zhou for their comments  
1356 and feedback.

1358

1359 This work benefited from earlier unpublished work by Laura Davies, Phil Reid, Andrew  
1360 G. Marshall.

1361

1362

1363 This research was undertaken with the assistance of resources from the National  
1364 Computational Infrastructure (NCI Australia), an NCRIS enabled capability supported  
1365 by the Australian Government.

1366

1367 This work was supported by ARC SRIEAS Grant SR200100005 Securing Antarctica's  
1368 Environmental Future.

1369

1370

## 1371 **Code and data availability**

1372

1373

1374 The underlying code for this study is available on GitHub:  
1375

1376 [https://github.com/eliocamp/access-s2\\_ice-eval](https://github.com/eliocamp/access-s2_ice-eval).

1377

1378

1379

1380

Raw data of ACCESS-S1 and ACCESS-S2 hindcast are not available due to size. Derived datasets required to reproduce the results, including extent time-series and error measures, are available in this Zenodo repository: <a href="https://zenodo.org/records/17479538">https://zenodo.org/records/17479538</a> <sup>48</sup>	1381 1382 1383 1384 1385 1386 1387 1388 1389 1390 1391 1392 1393 1394 1395 1396 1397 1398 1399 1400 1401 1402 1403 1404 1405 1406 1407 1408 1409 1410 1411 1412 1413 1414 1415 1416 1417 1418 1419 1420 1421 1422 1423 1424 1425 1426
<b>Competing interests</b>	All authors declare no financial or non-financial competing interests.
<b>Author contributions</b>	EC performed the data analysis and wrote the manuscript draft. AP, JA, EL, MW and PR, performed interpretation of the results, and reviewed and edited the draft. All authors read and approved the final manuscript.
<b>References</b>	[1] De Silva, L.W.A., Inoue, J., Yamaguchi, H., Terui, T.: Medium range sea ice prediction in support of Japanese research vessel MIRAI's expedition cruise in 2018. <i>Polar Geography</i> <b>43</b> (2-3), 223–239 (2020) <a href="https://doi.org/10.1080/1088937X.2019.1707317">https://doi.org/10.1080/1088937X.2019.1707317</a>
	[2] Wagner, P.M., Hughes, N., Bourbonnais, P., Stroeve, J., Rabenstein, L., Bhatt, U., Little, J., Wiggins, H., Fleming, A.: Sea-ice information and forecast needs for industry maritime stakeholders. <i>Polar Geography</i> <b>43</b> (2-3), 160–187 (2020) <a href="https://doi.org/10.1080/1088937X.2020.1766592">https://doi.org/10.1080/1088937X.2020.1766592</a>
	[3] Rinke, A., Maslowski, W., Dethloff, K., Clement, J.: Influence of sea ice on the atmosphere: A study with an Arctic atmospheric regional climate model. <i>Journal</i>

- 1427 of Geophysical Research: Atmospheres **111**(D16) (2006) <https://doi.org/10.1029/2005JD006957>
- 1428
- 1429
- 1430
- 1431 [4] Wang, Z., Fraser, A.D., Reid, P., Coleman, R., O'Farrell, S.: The Influence of  
1432 Time-Varying Sea Ice Concentration on Antarctic and Southern Ocean Numerical  
1433 Weather Prediction. *Weather and Forecasting* **39**(2), 293–310 (2024) <https://doi.org/10.1175/WAF-D-22-0220.1> . Chap. *Weather and Forecasting*
- 1434
- 1435
- 1436
- 1437
- 1438 [5] Semmler, T., Kasper, M.A., Jung, T., Serrar, S.: Remote impact of the Antarctic  
1439 atmosphere on the southern mid?latitudes. *Meteorologische Zeitschrift* **25**(1),  
1440 71–77 (2016) <https://doi.org/10.1127/metz/2015/0685>
- 1441
- 1442
- 1443
- 1444 [6] Zampieri, L., Goessling, H.F., Jung, T.: Predictability of Antarctic Sea Ice Edge  
1445 on Subseasonal Time Scales. *Geophysical Research Letters* **46**(16), 9719–9727  
1446 (2019) <https://doi.org/10.1029/2019GL084096>
- 1447
- 1448
- 1449
- 1450 [7] Gao, Y., Xiu, Y., Nie, Y., Luo, H., Yang, Q., Zampieri, L., Lv, X., Uotila,  
1451 P.: An Assessment of Subseasonal Prediction Skill of the Antarctic Sea Ice  
1452 Edge. *Journal of Geophysical Research: Oceans* **129**(11), 2024–021499 (2024)  
1453
- 1454
- 1455
- 1456
- 1457
- 1458 [8] Massonnet, F., Barreira, S., Barthélemy, A., Bilbao, R., Blanchard-Wrigglesworth,  
1459 E., Blockley, E., Bromwich, D.H., Bushuk, M., Dong, X., Goessling, H.F., Hobbs,  
1460 W., Iovino, D., Lee, W.-S., Li, C., Meier, W.N., Merryfield, W.J., Moreno-  
1461 Chamorro, E., Morioka, Y., Li, X., Niraula, B., Petty, A., Sanna, A., Scilingo, M.,  
1462 Shu, Q., Sigmond, M., Sun, N., Tietsche, S., Wu, X., Yang, Q., Yuan, X.: SIPN  
1463 South: Six years of coordinated seasonal Antarctic sea ice predictions. *Frontiers*  
1464 in Marine Science
- 1465 **10** (2023) <https://doi.org/10.3389/fmars.2023.1148899>
- 1466
- 1467
- 1468 [9] Dong, X., Yang, Q., Nie, Y., Zampieri, L., Wang, J., Liu, J., Chen, D.: Antarctic  
1469
- 1470
- 1471
- 1472

- sea ice prediction with A convolutional long short-term memory network. *Ocean Modelling* **190**, 102386 (2024) <https://doi.org/10.1016/j.ocemod.2024.102386> 1473  
 1474  
 1475  
 1476  
 1477  
 1478  
 1479  
 1480  
 1481  
 1482  
 1483  
 1484  
 1485  
 1486  
 1487  
 1488  
 1489  
 1490  
 1491  
 1492  
 1493  
 1494  
 1495  
 1496  
 1497  
 1498  
 1499  
 1500  
 1501  
 1502  
 1503  
 1504  
 1505  
 1506  
 1507  
 1508  
 1509  
 1510  
 1511  
 1512  
 1513  
 1514  
 1515  
 1516  
 1517  
 1518
- [10] Lin, Y., Yang, Q., Li, X., Dong, X., Luo, H., Nie, Y., Wang, J., Wang, Y., Min, C.: Ice-kNN-South: A Lightweight Machine Learning Model for Antarctic Sea Ice Prediction. *Journal of Geophysical Research: Machine Learning and Computation* **2**(1), 2024-000433 (2025) <https://doi.org/10.1029/2024JH000433>
- [11] Guemas, V., Chevallier, M., Déqué, M., Bellprat, O., Doblas-Reyes, F.: Impact of sea ice initialization on sea ice and atmosphere prediction skill on seasonal timescales. *Geophysical Research Letters* **43**(8), 3889–3896 (2016) <https://doi.org/10.1002/2015GL066626>
- [12] Day, J.J., Hawkins, E., Tietsche, S.: Will Arctic sea ice thickness initialization improve seasonal forecast skill? *Geophysical Research Letters* **41**(21), 7566–7575 (2014) <https://doi.org/10.1002/2014GL061694>
- [13] Holland, M.M., Blanchard-Wrigglesworth, E., Kay, J., Vavrus, S.: Initial-value predictability of Antarctic sea ice in the Community Climate System Model 3. *Geophysical Research Letters* **40**(10), 2121–2124 (2013) <https://doi.org/10.1002/grl.50410>
- [14] Marchi, S., Fichefet, T., Goosse, H.: Respective influences of perturbed atmospheric and ocean–sea ice initial conditions on the skill of seasonal Antarctic sea ice predictions: A study with NEMO3.6–LIM3. *Ocean Modelling* **148**, 101591 (2020) <https://doi.org/10.1016/j.ocemod.2020.101591>
- [15] Morioka, Y., Iovino, D., Cipollone, A., Masina, S., Behera, S.K.: Decadal Sea Ice Prediction in the West Antarctic Seas with Ocean and Sea Ice Initializations. *Communications Earth & Environment* **3**(1), 189 (2022) <https://doi.org/10.1038/s43247-022-00529-z>

- 1519 [16] Wedd, R., Alves, O., Burgh-Day, C., Down, C., Griffiths, M., Hendon, H.H.,  
1520 Hudson, D., Li, S., Lim, E.-P., Marshall, A.G., Shi, L., Smith, P., Smith, G.,  
1521 Spillman, C.M., Wang, G., Wheeler, M.C., Yan, H., Yin, Y., Young, G., Zhao, M.,  
1522 Xiao, Y., Zhou, X.: ACCESS-S2: The upgraded Bureau of Meteorology multi-week  
1523 to seasonal prediction system. *Journal of Southern Hemisphere Earth Systems*  
1524 *Science* **72**(3), 218–242 (2022) <https://doi.org/10.1071/ES22026>  
1525  
1526  
1527  
1528  
1529  
1530 [17] Hudson, D., Alves, O., Hendon, H.H., Lim, E.-P., Liu, G., Luo, J.-J., MacLachlan,  
1531 C., Marshall, A.G., Shi, L., Wang, G., Wedd, R., Young, G., Zhao, M., Zhou, X.:  
1532 ACCESS-S1 The new Bureau of Meteorology multi-week to seasonal prediction  
1533 system. *Journal of Southern Hemisphere Earth Systems Science* **67**(3), 132–159  
1534 (2017) <https://doi.org/10.1071/es17009>  
1535  
1536  
1537  
1538  
1539 [18] Williams, K.D., Harris, C.M., Bodas-Salcedo, A., Camp, J., Comer, R.E., Copsey,  
1540 D., Fereday, D., Graham, T., Hill, R., Hinton, T., Hyder, P., Ineson, S., Masato,  
1541 G., Milton, S.F., Roberts, M.J., Rowell, D.P., Sanchez, C., Shelly, A., Sinha, B.,  
1542 Walters, D.N., West, A., Woollings, T., Xavier, P.K.: The Met Office Global  
1543 Coupled model 2.0 (GC2) configuration. *Geoscientific Model Development* **8**(5),  
1544 1509–1524 (2015) <https://doi.org/10.5194/gmd-8-1509-2015>  
1545  
1546  
1547  
1548  
1549  
1550 [19] Waters, J., Bell, M.J., Martin, M.J., Lea, D.J.: Reducing ocean model imbalances  
1551 in the equatorial region caused by data assimilation. *Quarterly Journal of the Royal*  
1552 *Meteorological Society* **143**(702), 195–208 (2017) <https://doi.org/10.1002/qj.2912>  
1553  
1554  
1555  
1556 [20] Best, M.J., Pryor, M., Clark, D.B., Rooney, G.G., Essery, R.L.H., Ménard, C.B.,  
1557 Edwards, J.M., Hendry, M.A., Porson, A., Gedney, N., Mercado, L.M., Sitch,  
1558 S., Blyth, E., Boucher, O., Cox, P.M., Grimmond, C.S.B., Harding, R.J.: The  
1559 Joint UK Land Environment Simulator (JULES), model description – Part 1:  
1560 Energy and water fluxes. *Geoscientific Model Development* **4**(3), 677–699 (2011)  
1561  
1562  
1563  
1564

<a href="https://doi.org/10.5194/gmd-4-677-2011">https://doi.org/10.5194/gmd-4-677-2011</a>	1565
	1566
[21] Gurvan, M., Bourdallé-Badie, R., Bouttier, P.-A., Bricaud, C., Bruciaferri, D., Calvert, D., Chanut, J., Clementi, E., Coward, A., Delrosso, D., Ethé, C., Flavoni, S., Graham, T., Harle, J., Iovino, D., Lea, D., Lévy, C., Lovato, T., Martin, N., Masson, S., Mocavero, S., Paul, J., Rousset, C., Storkey, D., Storto, A., Vancoppenolle, M.: NEMO ocean engine (2013) <a href="https://doi.org/10.5281/zenodo.1475234">https://doi.org/10.5281/zenodo.1475234</a>	1567
	1568
	1569
	1570
	1571
	1572
	1573
	1574
	1575
	1576
	1577
[22] Megann, A., Storkey, D., Aksenov, Y., Alderson, S., Calvert, D., Graham, T., Hyder, P., Siddorn, J., Sinha, B.: GO5.0: The joint NERC–Met Office NEMO global ocean model for use in coupled and forced applications. Geoscientific Model Development <b>7</b> (3), 1069–1092 (2014) <a href="https://doi.org/10.5194/gmd-7-1069-2014">https://doi.org/10.5194/gmd-7-1069-2014</a>	1578
	1579
	1580
	1581
	1582
	1583
	1584
	1585
	1586
	1587
	1588
	1589
	1590
	1591
	1592
[23] Rae, J.G.L., Hewitt, H.T., Keen, A.B., Ridley, J.K., West, A.E., Harris, C.M., Hunke, E.C., Walters, D.N.: Development of the Global Sea Ice 6.0 CICE configuration for the Met Office Global Coupled model. Geoscientific Model Development <b>8</b> (7), 2221–2230 (2015) <a href="https://doi.org/10.5194/gmd-8-2221-2015">https://doi.org/10.5194/gmd-8-2221-2015</a>	1593
	1594
[24] Dee, D.P., Uppala, S.M., Simmons, A.J., Berrisford, P., Poli, P., Kobayashi, S., Andrae, U., Balmaseda, M.A., Balsamo, G., Bauer, P., Bechtold, P., Beljaars, A.C.M., van de Berg, L., Bidlot, J., Bormann, N., Delsol, C., Dragani, R., Fuentes, M., Geer, A.J., Haimberger, L., Healy, S.B., Hersbach, H., Hólm, E.V., Isaksen, L., Kållberg, P., Köhler, M., Matricardi, M., McNally, A.P., Monge-Sanz, B.M., Morcrette, J.-J., Park, B.-K., Peubey, C., de Rosnay, P., Tavolato, C., Thépaut, J.-N., Vitart, F.: The ERA-Interim reanalysis: Configuration and performance of the data assimilation system. Quarterly Journal of the Royal Meteorological Society <b>137</b> (656), 553–597 (2011) <a href="https://doi.org/10.1002/qj.828">https://doi.org/10.1002/qj.828</a>	1595
	1596
	1597
	1598
	1599
	1600
	1601
	1602
	1603
	1604
	1605
	1606
	1607
	1608
	1609
	1610

- 1611 [25] Waters, J., Lea, D.J., Martin, M.J., Mirouze, I., Weaver, A., While, J.: Imple-  
1612 menting a variational data assimilation system in an operational 1/4 degree global  
1613 ocean model. *Quarterly Journal of the Royal Meteorological Society* **141**(687),  
1614 333–349 (2015) <https://doi.org/10.1002/qj.2388>  
1615  
1616  
1617  
1618 [26] Good, S.A., Martin, M.J., Rayner, N.A.: EN4: Quality controlled ocean tem-  
1619 perature and salinity profiles and monthly objective analyses with uncertainty  
1620 estimates. *Journal of Geophysical Research: Oceans* **118**(12), 6704–6716 (2013)  
1621 <https://doi.org/10.1002/2013JC009067>  
1622  
1623  
1624  
1625 [27] Reynolds, R.W., Smith, T.M., Liu, C., Chelton, D.B., Casey, K.S., Schlax, M.G.:  
1626 Daily High-Resolution-Blended Analyses for Sea Surface Temperature. *Journal*  
1627 *of Climate* **20**(22), 5473–5496 (2007) <https://doi.org/10.1175/2007JCLI1824.1>.  
1628  
1629  
1630  
1631 Chap. *Journal of Climate*  
1632  
1633 [28] Zweng, M.M., Reagan, J.R., Antonov, J.I., Locarnini, R.A., Mishonov, A.V.,  
1634 Boyer, T.P., Garcia, H.E., Baranova, O.K., Johnson, D.R., Seidov, D., Biddle,  
1635 M.M.: *World ocean atlas 2013. Volume 2, Salinity* (2013) <https://doi.org/10.7289/V5251G4D>  
1636  
1637  
1638  
1639  
1640 [29] Meier, W.N., Stewart, J.S.: Assessing uncertainties in sea ice extent climate  
1641 indicators. *Environmental Research Letters* **14**(3), 035005 (2019) <https://doi.org/10.1088/1748-9326/aaf52c>  
1642  
1643  
1644  
1645  
1646 [30] Meier, W.N., Peng, G., Scott, D.J., Savoie, M.H.: Verification of a new NOAA/N-  
1647 SIDC passive microwave sea-ice concentration climate record. *Polar Research*  
1648  
1649 (2014) <https://doi.org/10.3402/polar.v33.21004>  
1650  
1651  
1652 [31] Cavalieri, D.J., Gloersen, P., Campbell, W.J.: Determination of sea ice parameters  
1653 with the NIMBUS 7 SMMR. *Journal of Geophysical Research: Atmospheres*  
1654  
1655  
1656

- 89**(D4), 5355–5369 (1984) <https://doi.org/10.1029/JD089iD04p05355> 1657  
1658
- [32] Comiso, J.: Bootstrap Sea Ice Concentrations from Nimbus-7 SMMR and DMSP SSM/I-SSMIS. (NSIDC-0079, Version 4). NASA National Snow and Ice Data Center Distributed Active Archive Center., Boulder, Colorado USA. (2023). <https://doi.org/10.5067/X5LG68MH013O> 1659  
1660  
1661  
1662  
1663  
1664  
1665  
1666  
1667  
1668  
1669  
1670  
1671  
1672  
1673  
1674  
1675  
1676  
1677  
1678  
1679  
1680  
1681  
1682  
1683  
1684  
1685  
1686  
1687  
1688  
1689  
1690  
1691  
1692  
1693  
1694  
1695  
1696  
1697  
1698  
1699  
1700  
1701  
1702
- [33] Meier, W.N., Fetterer, F., Windnagel, A.K., Stewart, J.S.: NOAA/NSIDC Climate Data Record of Passive Microwave Sea Ice Concentration. National Snow and Ice Data Center., Boulder, Colorado USA (2021). <https://doi.org/10.7265/efmz-2t65>
- [34] EUMETSAT Ocean and Sea Ice Satellite Application Facility: Global Sea Ice Concentration Climate Data Record 1978-2020 (v3.0, 2022), OSI-450-a, <https://cds.climate.copernicus.eu/cdsapp#!/dataset/satellite-sea-ice-concentration>
- [35] Cavalieri, D.J., Crawford, J.P., Drinkwater, M.R., Eppler, D.T., Farmer, L.D., Jentz, R.R., Wackerman, C.C.: Aircraft active and passive microwave validation of sea ice concentration from the Defense Meteorological Satellite Program special sensor microwave imager. *Journal of Geophysical Research: Oceans* **96**(C12), 21989–22008 (1991) <https://doi.org/10.1029/91JC02335>
- [36] Murphy, A.H., Daan, H.: Forecast Evaluation. In: *Probability, Statistics, And Decision Making In The Atmospheric Sciences*. CRC Press, ??? (1985)
- [37] R Core Team: R: A Language and Environment for Statistical Computing. R Foundation for Statistical Computing, Vienna, Austria (2020). R Foundation for Statistical Computing
- [38] Dowle, M., Srinivasan, A.: Data.Table: Extension of 'Data.Frame' (2020)
- [39] Campitelli, E.: metR: Tools for Easier Analysis of Meteorological Fields (2020)

- 1703 [40] Schulzweida, U.: CDO User Guide (2023) <https://doi.org/10.5281/ZENODO.10020800>
- 1704  
1705  
1706  
1707 [41] Wickham, H.: Ggplot2: Elegant Graphics for Data Analysis. Use R! Springer,  
1708  
1709 New York (2009). <https://doi.org/10.1007/978-0-387-98141-3>
- 1710  
1711 [42] Xie, Y.: Dynamic Documents with R and Knitr, 2nd edn. Chapman and Hall/CRC,  
1712  
1713 Boca Raton, Florida (2015)
- 1714  
1715 [43] Allaire, J.J., Teague, C., Xie, Y., Dervieux, C.: Quarto. Zenodo (2022). <https://doi.org/10.5281/ZENODO.5960048>
- 1716  
1717  
1718  
1719 [44] Libera, S., Hobbs, W., Klocker, A., Meyer, A., Matear, R.: Ocean-Sea Ice  
1720 Processes and Their Role in Multi-Month Predictability of Antarctic Sea Ice.  
1721  
1722 Geophysical Research Letters **49**(8), 2021–097047 (2022) <https://doi.org/10.1029/2021GL097047>
- 1723  
1724  
1725  
1726  
1727 [45] Roach, L.A., Dörr, J., Holmes, C.R., Massonnet, F., Blockley, E.W., Notz, D.,  
1728 Rackow, T., Raphael, M.N., O'Farrell, S.P., Bailey, D.A., Bitz, C.M.: Antarctic  
1729 Sea Ice Area in CMIP6. Geophysical Research Letters **47**(9), 2019–086729 (2020)  
1730  
1731 <https://doi.org/10.1029/2019GL086729>
- 1732  
1733  
1734  
1735 [46] Zhou, X., Alves, O.: Evaluating sea ice in ACCESS-S2. Technical report, Bureau  
1736 of Meteorology (2022)
- 1737  
1738  
1739 [47] Bunzel, F., Notz, D., Baehr, J., Müller, W.A., Fröhlich, K.: Seasonal climate  
1740 forecasts significantly affected by observational uncertainty of Arctic sea ice  
1741 concentration. Geophysical Research Letters **43**(2), 852–859 (2016) <https://doi.org/10.1002/2015GL066928>
- 1742  
1743  
1744  
1745  
1746 [48] Campitelli, E.: Data for "Evaluating the Importance of Initial Conditions for  
1747  
1748

Antarctic Sea Ice Seasonal Predictability with a Fully Coupled Forecast Model".	1749
Zenodo (2025). <a href="https://doi.org/10.5281/ZENODO.17479537">https://doi.org/10.5281/ZENODO.17479537</a>	
	1750
	1751
	1752
	1753
	1754
	1755
	1756
	1757
	1758
	1759
	1760
	1761
	1762
	1763
	1764
	1765
	1766
	1767
	1768
	1769
	1770
	1771
	1772
	1773
	1774
	1775
	1776
	1777
	1778
	1779
	1780
	1781
	1782
	1783
	1784
	1785
	1786
	1787
	1788
	1789
	1790
	1791
	1792
	1793
	1794

1795 **Supplementary figures**

1796

1797

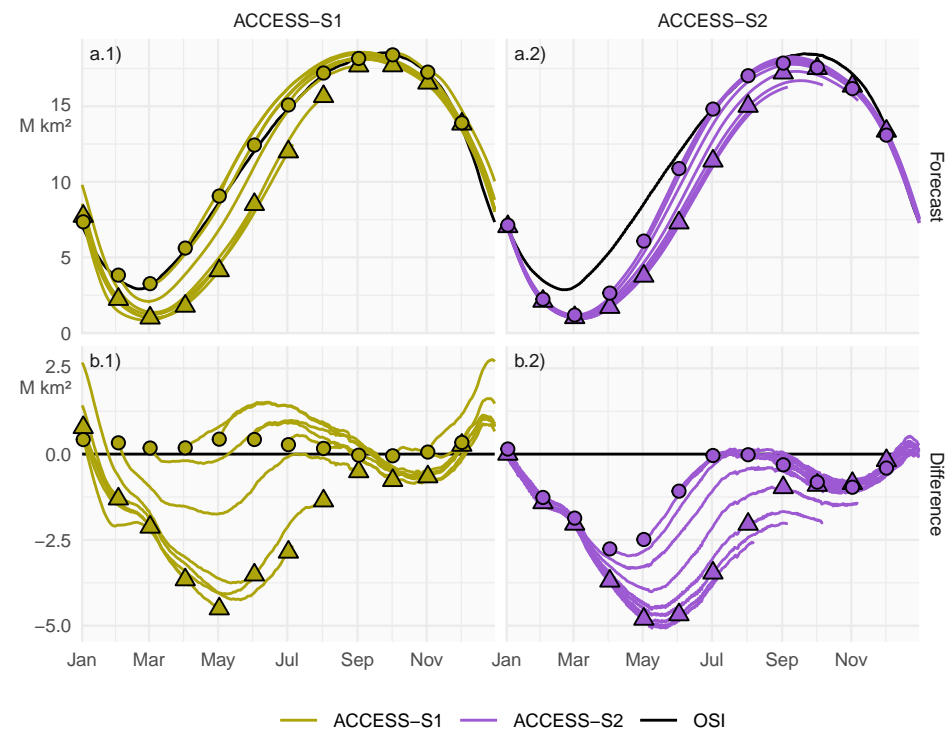
1798 The following are the same figures from the main paper but using the OSI dataset  
 1799 instead of CDR.

1800

1801

1802

1803



1826 **Figure A1:** Row a: Pan-Antarctic daily mean sea-ice extent for all hindcasts initialised  
 1827 on the first of each calendar month for ACCESS-S1 (column 1; green) and ACCESS-S2  
 1828 (column 2; purple). Observed mean sea-ice extent in each corresponding hindcast period  
 1829 is shown in black. Row b: Mean differences between the forecast and the observed  
 1830 values. Circles represent the initial conditions at the start of forecasts (i.e., the first of  
 1831 every month), and triangles represent the mean values at the lead time corresponding  
 1832 to the maximum lead time in S1 (between 213 and 216 days, depending on the month)

1833

1834

1835

1836

1837

1838

1839

1840

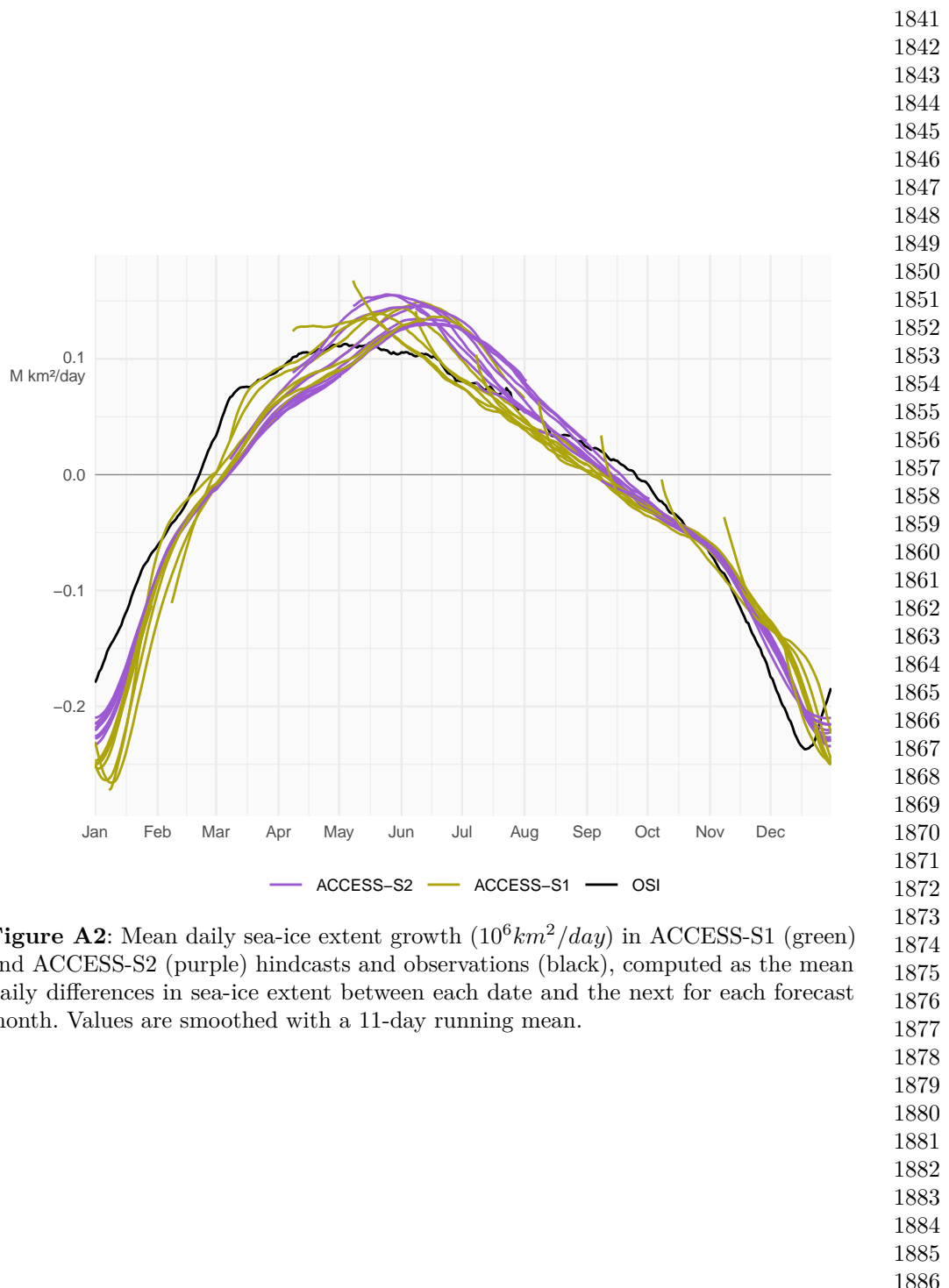


**Figure A2:** Mean daily sea-ice extent growth ( $10^6 \text{ km}^2/\text{day}$ ) in ACCESS-S1 (green) and ACCESS-S2 (purple) hindcasts and observations (black), computed as the mean daily differences in sea-ice extent between each date and the next for each forecast month. Values are smoothed with a 11-day running mean.

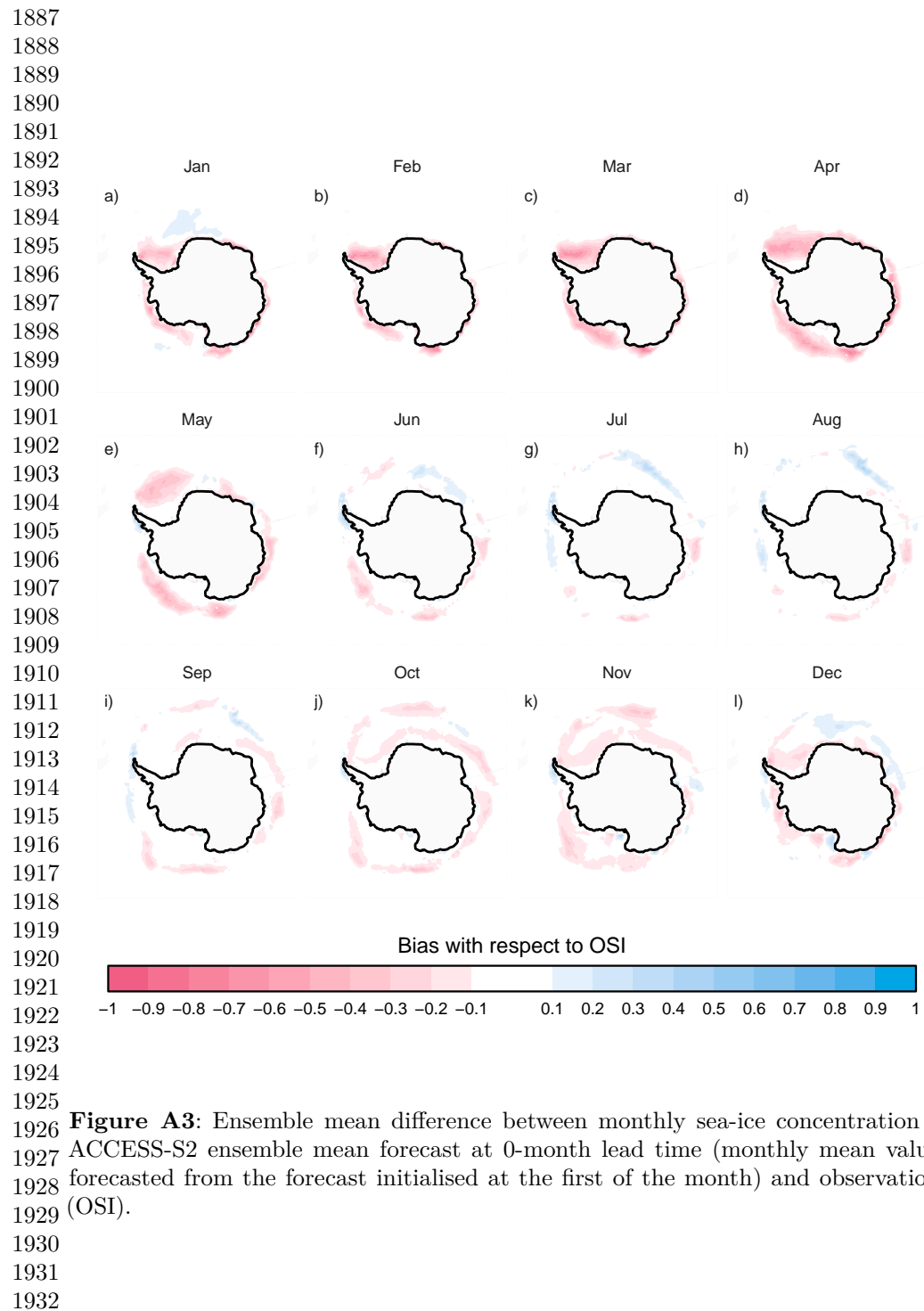


**Figure A3:** Ensemble mean difference between monthly sea-ice concentration of ACCESS-S2 ensemble mean forecast at 0-month lead time (monthly mean values forecasted from the forecast initialised at the first of the month) and observations (OSI).

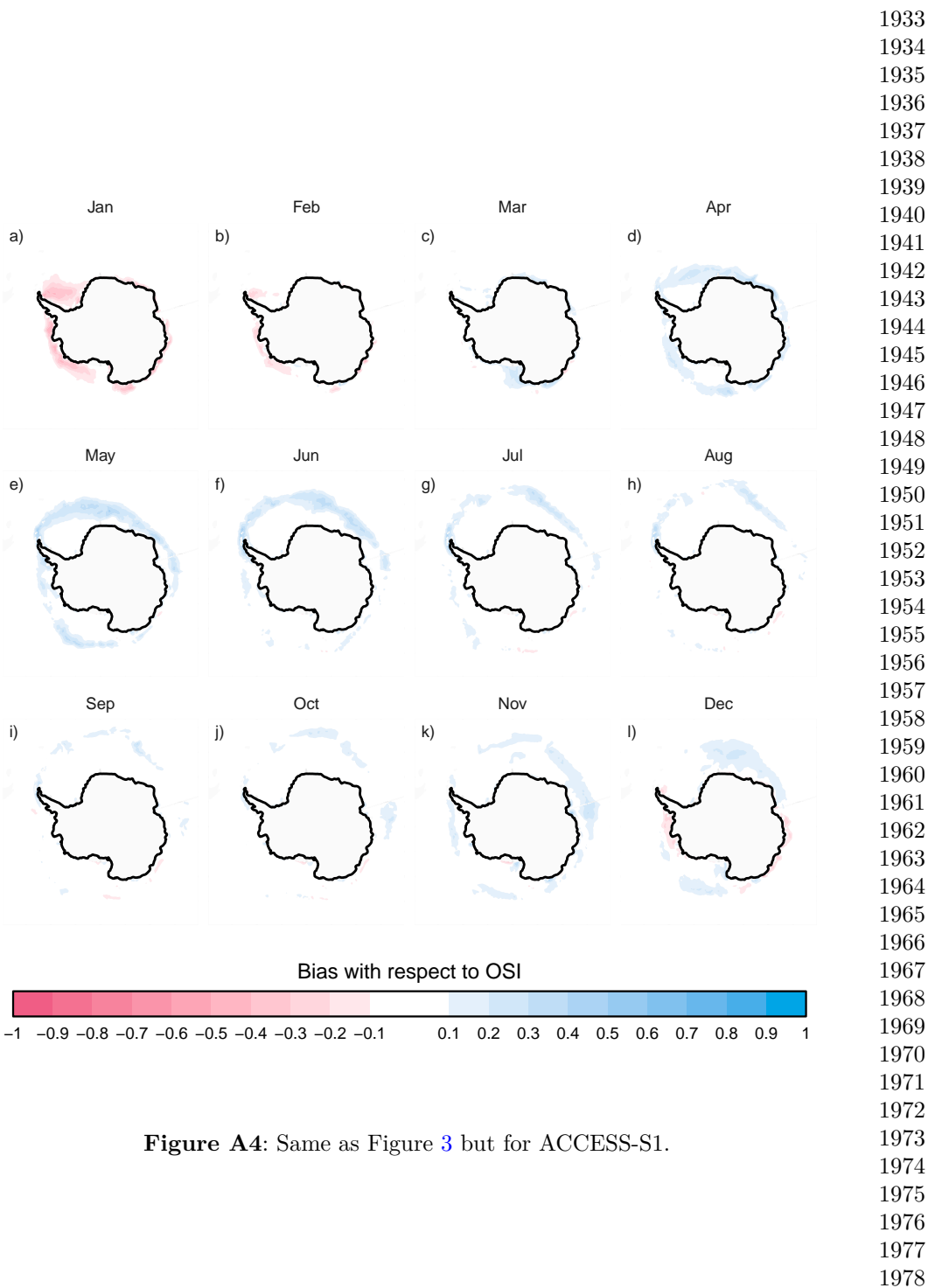


**Figure A4:** Same as Figure 3 but for ACCESS-S1.

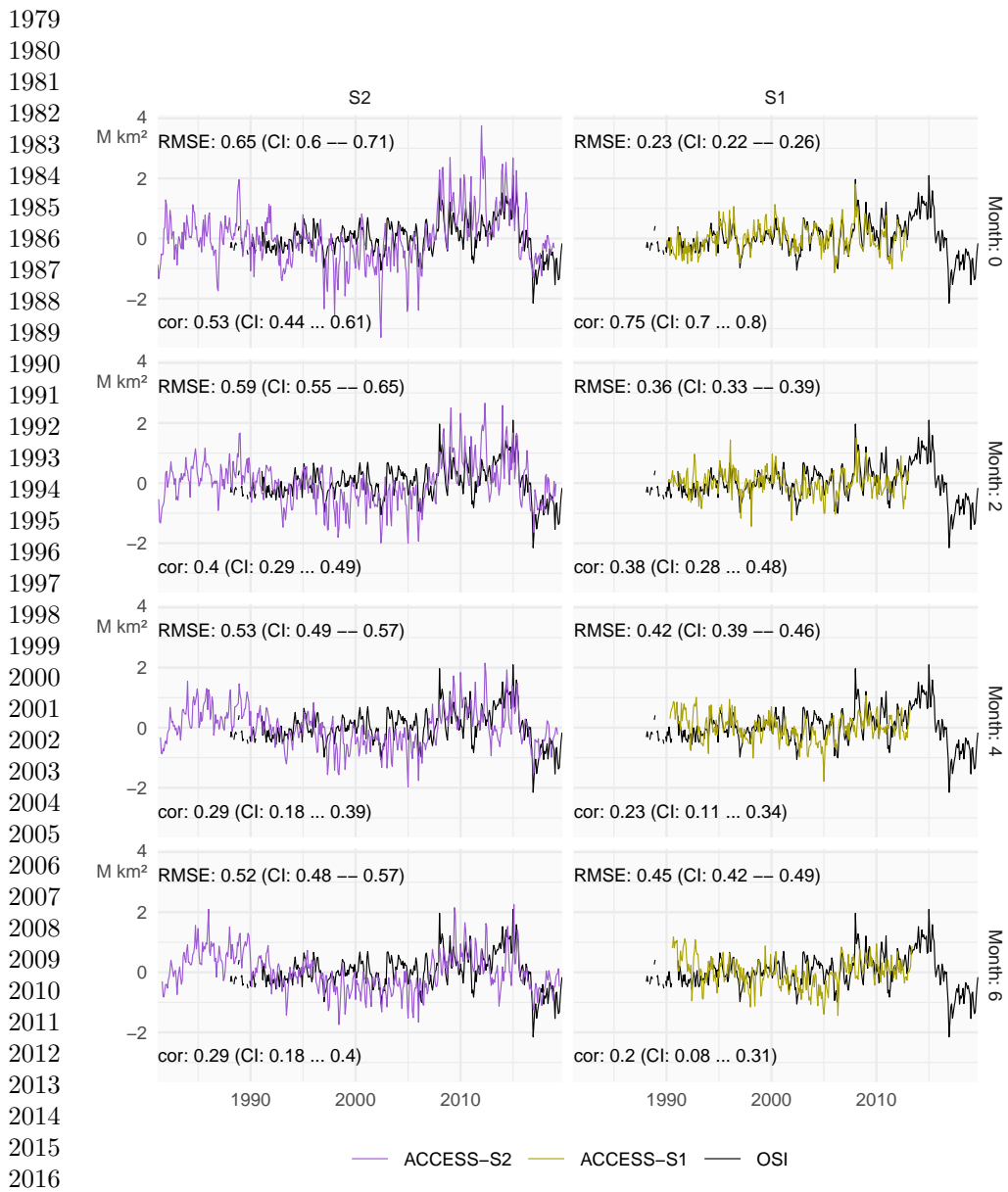


**Figure A5:** Monthly mean sea-ice extent anomalies of the observations (black) and forecasts from ACCESS-S1 (right column; purple) and ACCESS-S2 (left column; green) at lead times of 0, 2, 4, and 6 months. The RMSE and correlation during the overlapping period of ACCESS-S1 and ACCESS-S2 hindcasts (1990–2013) are shown on the top left and bottom left of each panel respectively.

2022  
2023  
2024

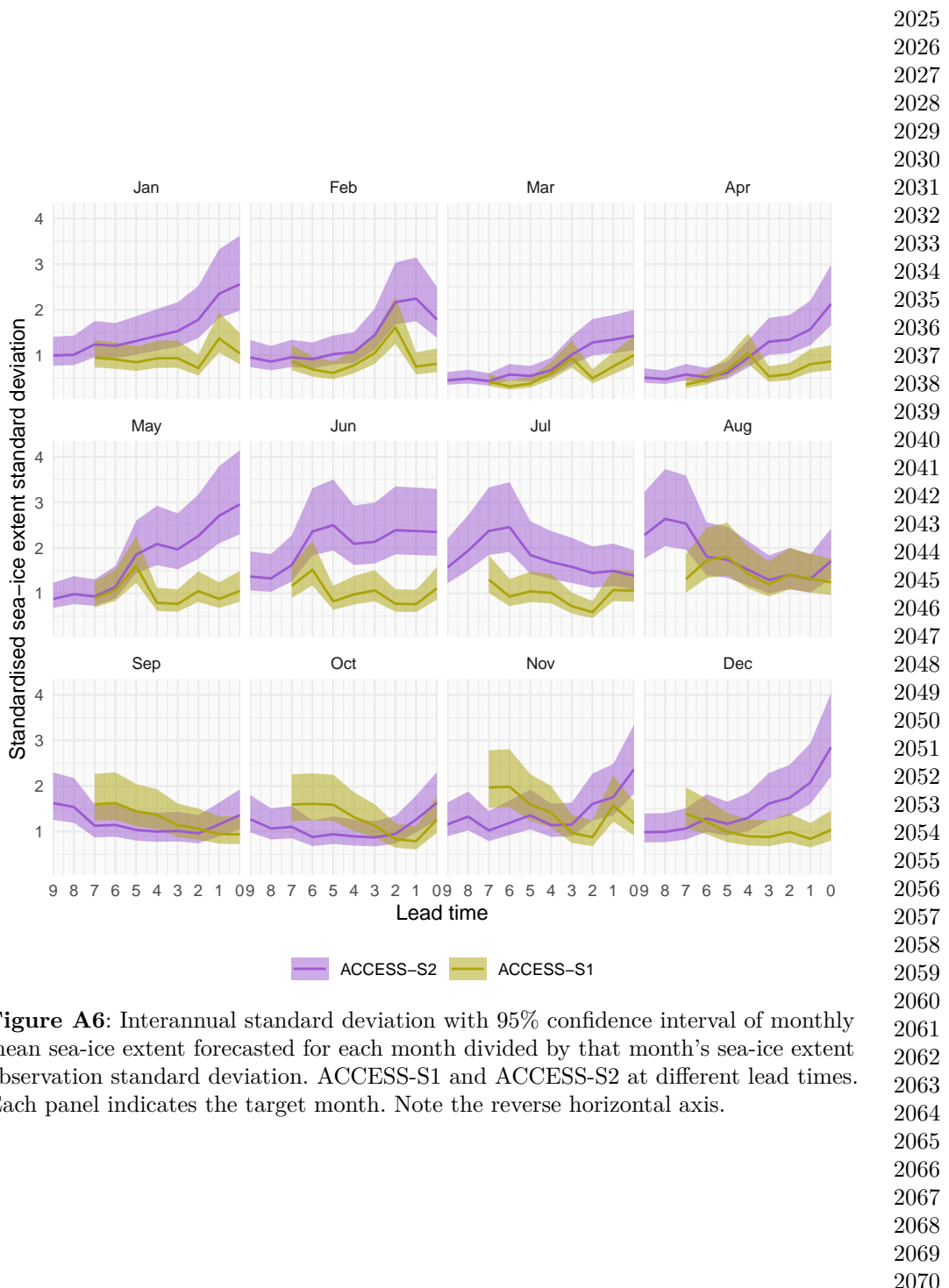


**Figure A6:** Interannual standard deviation with 95% confidence interval of monthly mean sea-ice extent forecasted for each month divided by that month's sea-ice extent observation standard deviation. ACCESS-S1 and ACCESS-S2 at different lead times. Each panel indicates the target month. Note the reverse horizontal axis.

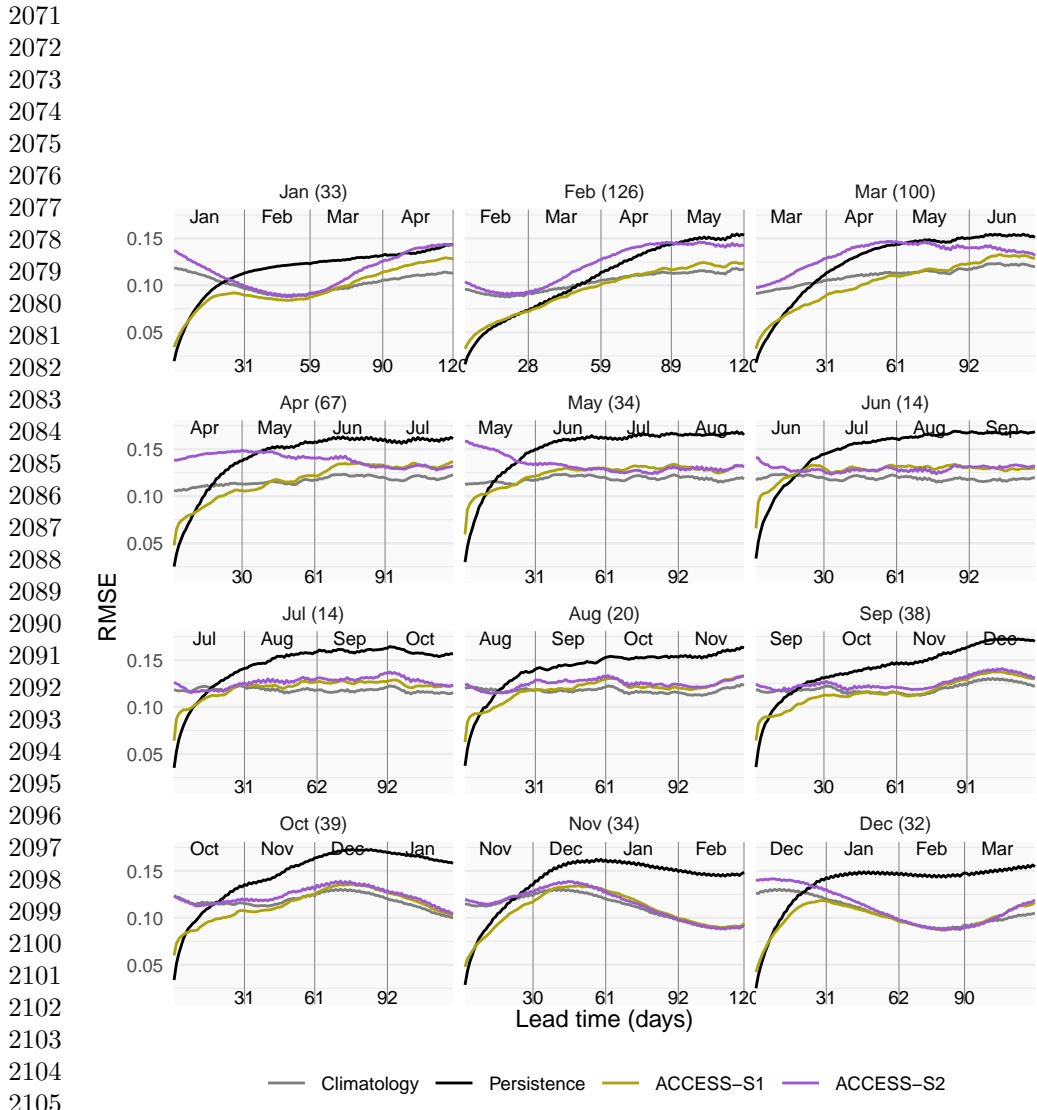


**Figure A7:** Mean RMSE of sea-ice concentration anomalies as a function of forecast lead time for all forecasts initialised on the first of each month compared with a reference forecast of persistence of anomalies (black) and climatology (gray). Only the first 120 days are shown. In parentheses, the shortest time at which ACCESS-S1 and ACCESS-S2 mean RMSE is not statistically different at the 99% confidence level.

2106  
2107  
2108  
2109  
2110  
2111  
2112  
2113  
2114  
2115  
2116

2117  
 2118  
 2119  
 2120  
 2121  
 2122  
 2123  
 2124  
 2125  
 2126  
 2127  
 2128  
 2129  
 2130  
 2131  
 2132  
 2133  
 2134  
 2135  
 2136  
 2137  
 2138  
 2139  
 2140  
 2141  
 2142  
 2143  
 2144  
 2145  
 2146  
 2147  
 2148  
 2149  
 2150  
 2151  
 2152  
 2153  
 2154  
 2155  
 2156  
 2157  
 2158  
 2159  
 2160  
 2161  
 2162

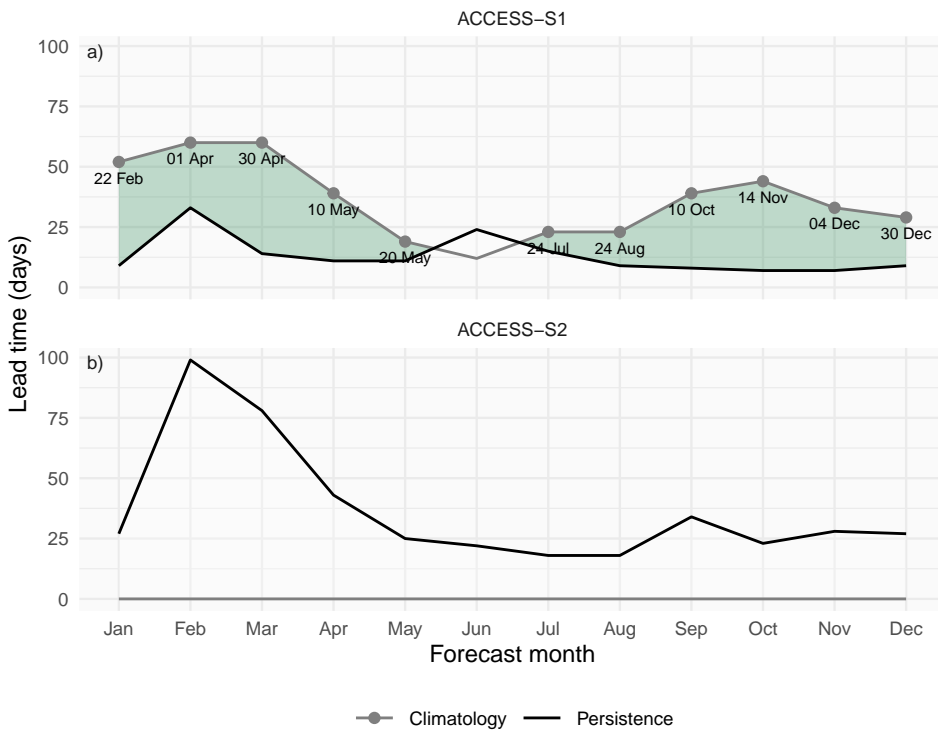
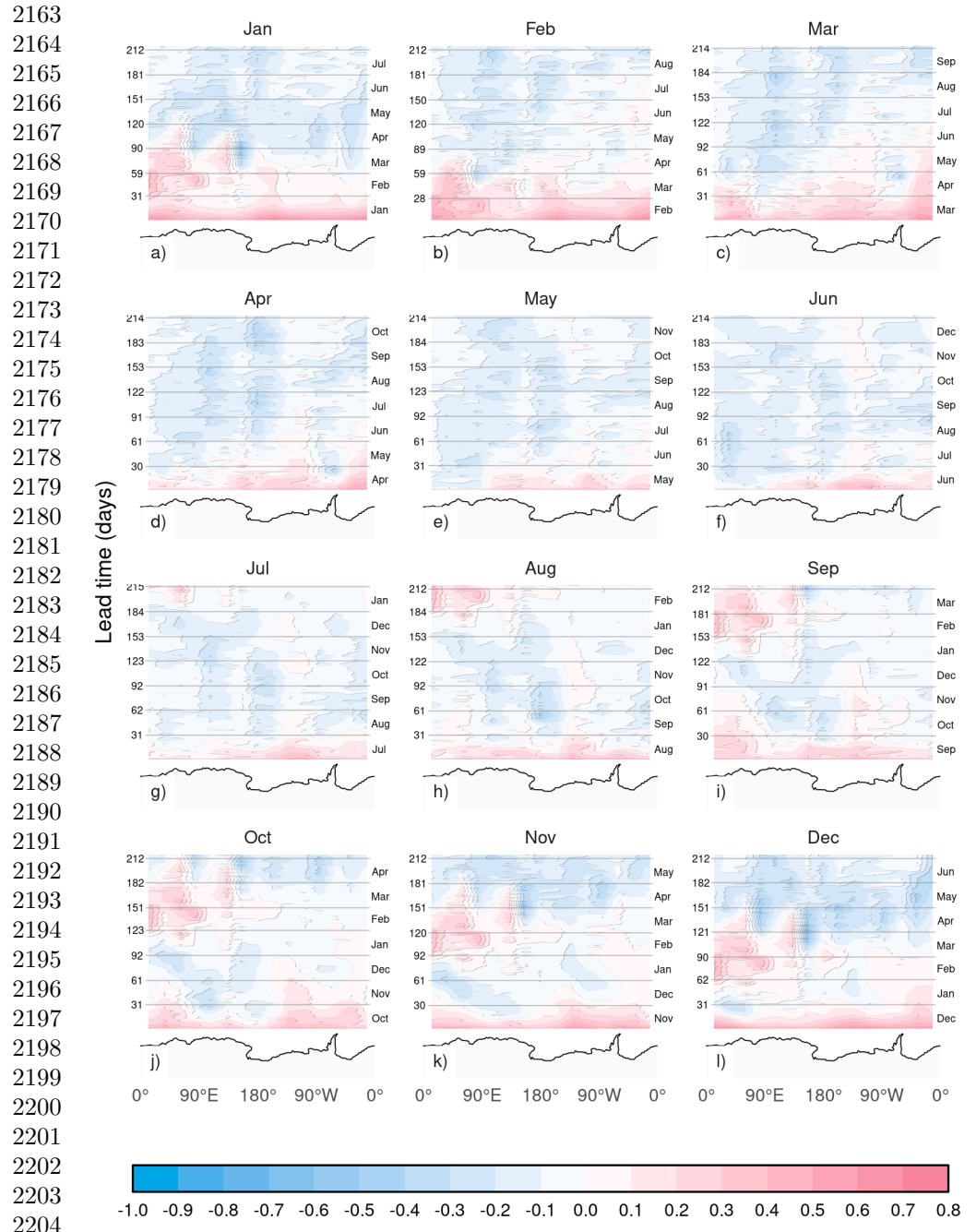


**Figure A8:** Minimum lead time at which each forecast's mean RMSE becomes larger than the lower bound of the 95% confidence interval of persistence forecast RMSE (black lines) and maximum lead time at which each forecast's mean RMSE remains lower than the lower bound of the 95% confidence interval of climatological forecast RMSE (gray lines). Green shading indicates the window where forecasts outperform both persistence (lead times longer than black line) and climatology (lead times shorter than gray line). Text labels show the date corresponding to the maximum lead time at which each forecast outperforms climatology.



2205 **Figure A9:** RMSE skill score of ACCESS-S1 forecasts with climatological forecast as  
 2206 reference computed on 15 meridional slices 24° wide as a function of lead time and  
 2207 longitude. Antarctica's coastline is shown at the bottom of each panel for reference.  
 2208

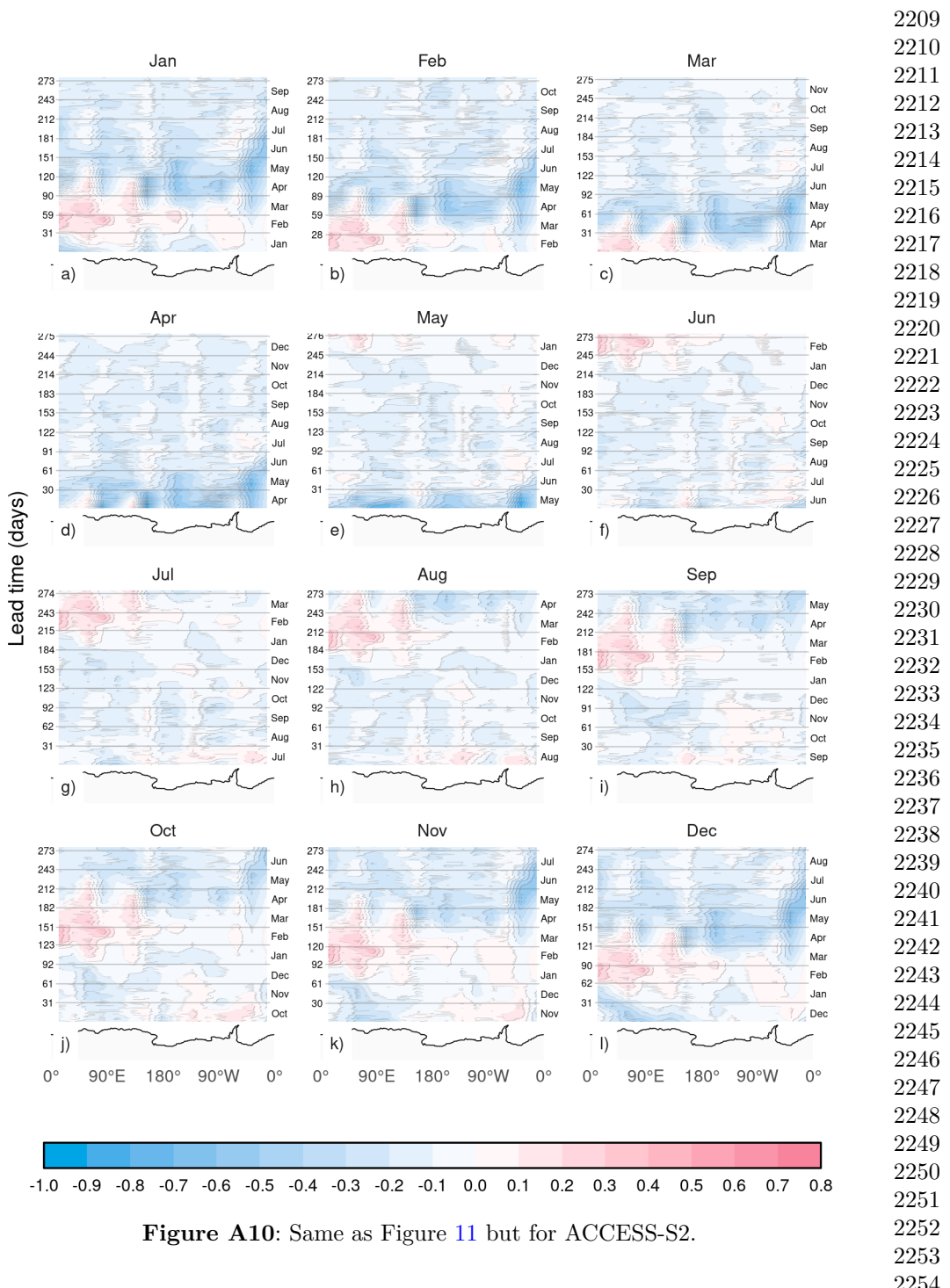


**Figure A10:** Same as Figure 11 but for ACCESS-S2.

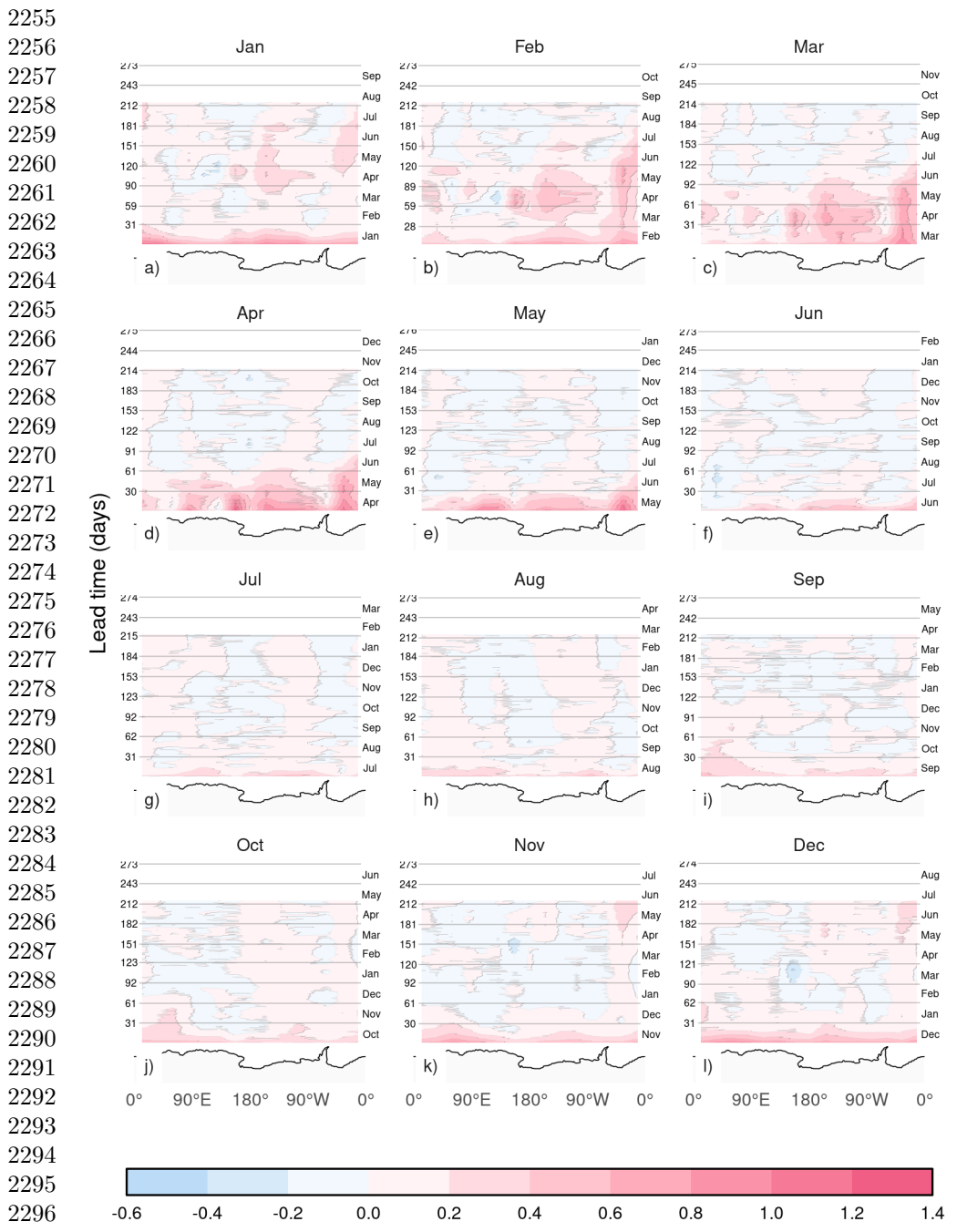


**Figure A11:** Same as Figure 11 but for the difference between ACCESS-S1 and ACCESS-S2.

2300

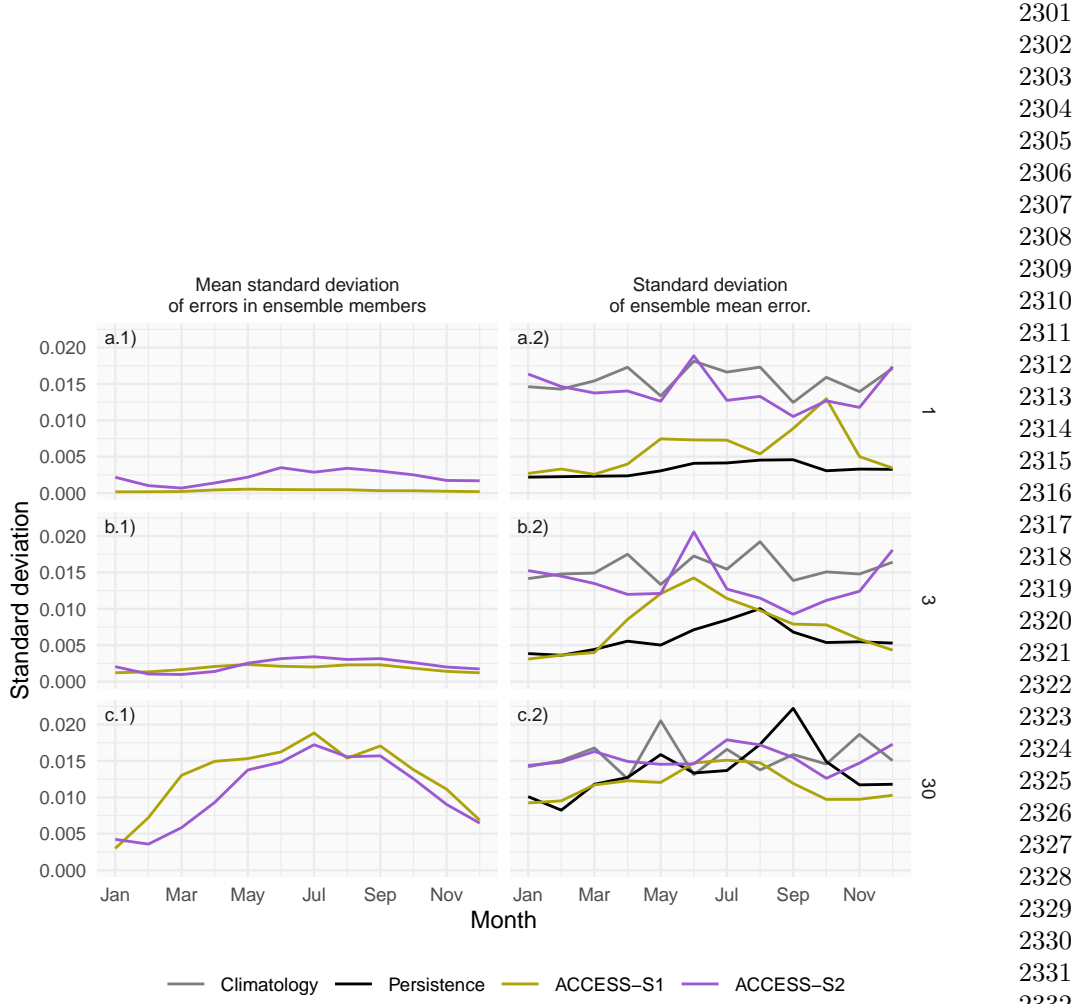


**Figure A12:** Decomposition of forecast error spread at 1, 5 and 30 days lead time for ACCESS-S1 and ACCESS-S2 hindcasts across initialization months. The left column shows the mean standard deviation of RMSE errors across ensemble members, while the right column shows the standard deviation of the ensemble mean RMSE error and the spread of the persistence and climatology forecasts errors.